Economic Geology, v. 103, pp. 1531–1562

Rhyolite Geochemical Signatures and Association with Volcanogenic Massive Sulfide Deposits: Examples from the Abitibi Belt, Canada

Damien Gaboury†

Université du Québec à Chicoutimi, Centre d'études sur les ressources minérales (CERM) and Consortium de recherche en exploration minérale (CONSOREM), 555 boul. de l'Université, Chicoutimi, Québec, Canada G7H 2B1

and Vital Pearson*

Consortium de recherche en exploration minérale (CONSOREM), 555 boul. de l'Université, Chicoutimi, Québec, Canada G7H 2B1

Abstract

The relationship between rhyolite geochemistry and volcanogenic massive sulfide (VMS) mineralization has been proposed as an exploration tool to discriminate prospective felsic volcanic centers. The most widely used classification discriminates between four types of rhyolite: FI, FII, FIIIa, and FIIIb. The FI rhyolites are calc-alkaline, with strongly fractionated REE patterns and strongly negative Ta and Nb anomalies. They are usually considered barren, unless associated with FII or FIII felsic volcanic rocks. The FII rhyolites are calc-alkaline to transitional with moderately fractionated REE patterns and moderate Ta and Nb anomalies. They range from barren to having a high potential to host VMS mineralization. The FIIIa and FIIIb rhyolites are tholeiitic and show weakly fractionated REE patterns and weak to absent Nb and Ta anomalies. They have the highest potential to host VMS mineralization. The FIIIb rhyolites are high-temperature rhyolites with flat REE patterns and no Ta or Nb anomalies.

The Abitibi greenstone belt, especially in Quebec, is well known for its abundant and diverse VMS deposits. Representative samples of VMS-associated rhyolites within and outside of mining districts, including the classic Noranda VMS district, were analyzed for major and trace elements to validate their proposed favorability for hosting VMS deposits. Results indicate that all of the rhyolite types are prospective, but mineralization may differ from the classic Noranda-type VMS deposit. The FI-type rhyolites appear to be particularly associated with gold-rich VMS deposits, such as the world-class Laronde deposit, and are more prospective for Cu-Au replacement and vein-type deposits. The FII-type rhyolites account for about 70 percent of rhyolites in the Abitibi belt. Although considered less prospective, some districts dominated by FII rhyolites, such as Val-d'Or and Selbaie, have collectively produced in excess of 100 million metric tons (Mt) of ore. Deposits in these districts mainly consist of sulfide veins and disseminated ore with low Cu and Zn grades and are associated with abundant and highly vesicular volcaniclastic rocks that display a compositional continuum from andesite to rhyolite. Other weakly mineralized FII districts (e.g., Hunter mine, Gemini-Turgeon) are characterized instead by bimodal flow-dome sequences. The FIIIa-type rhyolites occur mainly in the Noranda district and form flow-dome complexes in bimodal sequences with associated Noranda-type VMS mineralization. In small felsic centers (Joutel, Normétal, Chibougamau, Quévillon) that show a volcanic evolution from FIIIa to FII to FI affinities, VMS deposits are directly associated with FIIIa rhyolites, thus demonstrating the usefulness of rhyolite geochemistry for exploration in these areas. The FIIIb rhyolites are rare in the Abitibi belt, with most occurring in the Matagami district where they are associated with Zn-Cu VMS deposits. Based on this analysis, we suggest that a combination of rhyolite geochemistry, volcanic facies, and style of the mineralization may be more meaningfully applied in exploration than rhyolite type alone, particularly in the case of FI and FII rhyolites.

Introduction

For more than 25 years, the association between specific rhyolite suites and volcanogenic massive sulfide (VMS) deposits was promoted as an effective tool for exploration. Thurston (1981) and Campbell et al. (1982) first identified this relationship using Archean VMS deposits in the Canadian Shield. Lesher et al. (1986) and Barrie et al. (1993) subsequently developed formal classifications for felsic volcanic rocks based on trace element concentrations and suggested that certain types of rhyolites were more prospective for VMS deposits than others. Recently, Hart et al. (2004) revitalized the concept by proposing a conceptual petrogenetic model to account for the association of specific rhyolite geochemical signatures with VMS deposits. The classification geochemically discriminates rhyolites as FI, FII, FIIIa, or FIIIb types. The general conclusions drawn from Lesher et al. (1986), Lentz (1998), and Hart et al. (2004) are that Archean VMS deposits are hosted mainly by FIII rhyolites, whereas most post-Archean VMS deposits are hosted predominantly by FII rhyolites, and FI rhyolites are unfavorable for VMS mineralization. The link between VMS formation (hydrothermal activity) and rhyolite petrogenesis invokes a particular geodynamic setting and, more specifically, the depth of rhyolite generation (Lentz 1998; Hart et al., 2004).

Although exceptions and limitations were recognized, the concept was rapidly adopted by exploration companies, and rhyolites with the most potential were commonly selected without any consideration for the mineral potential of other

† Corresponding author: e-mail, dgaboury@uqac.ca

*Present address: Mines Virginia Inc., 116 St-Pierre, Suite 200, Québec, Québec, Canada G1K 4A7.

rhyolites in the vicinity. Recently, the discovery of the world-class, gold-rich VMS Laronde deposit in FI and FII rhyolites (Mercier-Langevin et al., 2007a, b) raised some doubt about the application of rhyolite classification in VMS exploration.

The Archean Abitibi belt is one of the most prolific VMS belts in the world (Rodney et al., 2002), hosting various types of VMS and volcanogenic gold deposits. Consequently, this belt constitutes an ideal laboratory for testing the validity of rhyolite classification as a means for finding ore deposits. In this paper, we reassess the use of rhyolite classification as an exploration tool in the Abitibi greenstone belt and present a compilation of the characteristics of ore-hosting rocks, alteration types, and volcanic facies. Felsic volcanic rocks in and around VMS districts in the Abitibi belt of Quebec were sampled and analyzed for major and trace elements. Rhyolites were classified using the parameters of Hart et al. (2004) and compared with VMS tonnages, mineralization type, and volcanic rock characteristics. This approach permits a semiquantitative comparison of the favorability of various rhyolite types.

Geology of the Abitibi Belt

The Abitibi greenstone belt in Canada (Fig. 1) is the largest and best preserved Archean belt (Card, 1990) and also one of the richest VMS-bearing belts in the world (Rodney et al., 2002). These include syngenetic VMS and gold-rich VMS deposits, as well as sulfide-rich, gold-bearing quartz veins and Cu-Au–bearing sulfide veins. All are genetically associated with felsic volcanic complexes (e.g., Chartrand and Cattalani, 1990). The Abitibi belt includes three of the world's largest and richest VMS deposits (>50 Mt of ore)—Kidd Creek, Horne, and Laronde—of which the last two are gold rich. Eight other large deposits (>15 Mt) also have been mined: Selbaie, Mattagami Lake, Bouchard-Hébert, Louvicourt, East Sullivan, Bousquet-1, Dumagami-Bousquet-2, and Quémont. Overall, more than 80 deposits are known, totaling more than 675 Mt of metallurgically high-quality Cu ± Zn ± Ag ± Au ore (Hannington et al., 1999a; Rodney et al., 2002).

The Abitibi greenstone belt is a linear east-trending volcano-sedimentary sequence intruded by plutonic suites (Fig. 1). It is thought to have developed through arc formation, arc evolution, arc-arc collision, and arc fragmentation dating from 2735 to 2670 Ma (Mueller et al., 1996; Daigneault et al., 2004). Wyman et al. (2002) proposed that the Abitibi-Wawa greenstone belt is the product of subduction tectonics, enhanced and modified by mantle plume interaction. The belt is broadly divided into the 2735 to 2705 Ma North Volcanic zone and the 2715 to 2697 Ma Southern Volcanic zone (Chown et al. 1992), although more recent compilations present a more complex evolution (e.g., Ayer et al., 2003, 2005; Goutier and Melancon, 2007). The east-trending Porcupine-Destor-Manneville fault separates the Northern and Southern Volcanic zones, and the Cadillac-Larder Lake fault defines the southern boundary of the Southern Volcanic zone (Fig. 1). In addition, the North Volcanic zone is also divided into external (NVZ-ext) and internal (NVZ-int) segments (Fig. 1) separated by the linear, east-trending Chicobi sedimentary sequence (Daigneault et al., 2004).

Three main volcanic cycles are recognized in the Quebec segment (Daigneault et al., 2004). Cycle 1, from 2735 to 2720 Ma, corresponds to a subaqueous basaltic plain punctuated by several isolated felsic centers, such as Joutel, Normétal, Matagami, Gemini, Selbaie, Hunter, and Chibougamau (Lemoine). All these felsic centers have well-documented synvolcanic intrusions (Gaboury, 2006), felsic domes and lavas, and associated VMS mineralization. Cycle 2, from 2720 to 2705 Ma, is interpreted as an emerging and evolving arc, to which some synvolcanic plutons have been linked (Chown et al., 1992), such as the Chibougamau pluton with its Cu-Au vein-type deposits, the Kamiskotia pluton (Barrie and Davis, 1990) with VMS deposits in associated felsic lavas, and the Mountain pluton, which has been indirectly dated at 2718 Ma based on the age of cogenetic felsic lavas at the Langlois VMS mine (Davis et al., 2005). The 2717 to 2711 Ma rhyolites at Kidd Creek (Bleeker et al., 1999) are compositionally distinct from these other cycle 2 felsic rocks due to their high silica contents and their REE-HFSE patterns comparable to rhyolites from the Iceland rift zone (Prior et al., 1999). The Kidd Creek VMS deposit is also exceptional due to its size and metal content (Hannington et al., 1999a), as well as the apparent lack of an association with a synvolcanic intrusion (Barrie et al., 1999). Cycle 3 is restricted to the Southern Volcanic zone and is interpreted as arc volcanism (e.g., Daigneault et al., 2004). The Southern Volcanic zone includes the Blake River Group (2703–2698 Ma) and the Malartic segment (2714–2701 Ma). The Blake River is thought to represent the development of a multiphase megacaldera, recently proposed by Pearson and Daigneault (2009), which hosts major VMS deposits associated with three main synvolcanic intrusions, the Flavrian-Powell, Cléricy, and Mooshla intrusions and associated felsic rocks. The Malartic segment has recorded a complex evolution (Scott et al., 2002) involving komatiitic rifting at the base (2714 Ma) followed by arc evolution and later arc rifting (2705–2701). The VMS deposits of the Val-d'Or mining district occur specifically in the arc-related volcanic sequence (Scott et al., 2002) associated with the synvolcanic Bourlamaque pluton (Fig. 1).

Daigneault et al. (2004) determined that the deformation history is diachronous: 2710 to 2690 Ma in the North Volcanic zone and 2698 to 2640 Ma in the Southern Volcanic zone but following the same pattern for both. In each case, the first phase consisted of north-south deformation dominated by shortening that induced thrusting along major east-trending boundary faults (the Porcupine-Destor-Manneville and Cadillac-Larder Lake faults), folding, and the development of a regional east-trending schistosity. The second phase was a dextral, transpressional late-stage increment responsible for dextral movement along major east-trending faults (the Destor-Manneville and Cadillac-Larder Lake faults) and the development of a southeast-trending fault system. Syntectonic intrusions were emplaced locally during all stages of the deformation history. As a consequence of this structural evolution, VMS-hosting sequences or districts occur as (1) monoclinal laterally extensive and tilted sequences located stratigraphically above their synvolcanic pluton, as exemplified by the Normétal, Val-d'Or, Bousquet, Selbaie, Chibougamau (Lemoine), Langlois, and Gemini mining districts; (2) as sequences occurring on both flanks of an anticline centered on a synvolcanic intrusion, such as those found in the Noranda, Matagami, and Hunter districts; or (3) as a complexly folded sequence, such as the Joutel district.

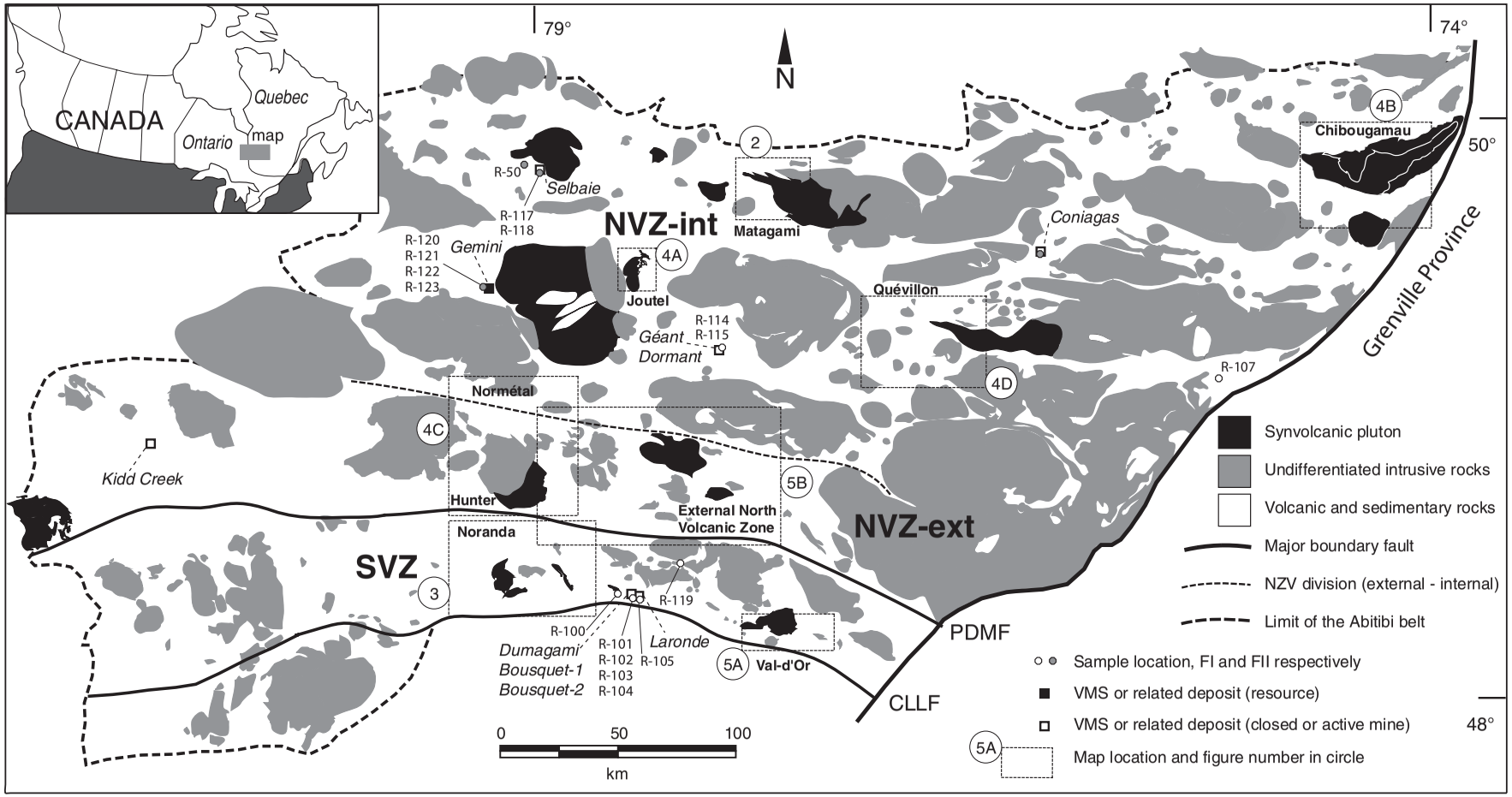

FIG. 1. Simplified geologic map of the Abitibi belt, showing the locations of VMS and volcanogenic deposits considered in this study. Locations of samples outside detailed sample areas are shown (see Figs. 2–5 for enlargements of detailed sample areas). Major subdivisions are the Southern Volcanic zone (SVZ), the external North Volcanic zone (NVZ-ext), and internal North Volcanic zone (NVZ-int). Major faults are the Porcupine-Destor-Manneville fault (PDMF) and the Cadillac-Larder Lake fault (CLLF). Map modified from Chown et al. (1992), Daigneault et al. (2004), and Gaboury (2006).

Methodology

Sampling

During the summer of 2003, more than 120 felsic rocks (mainly rhyolite with minor quantities of dacite) were sampled from outcrop, with another four taken from drill cores (App. 1; Figs. 1–5). Four samples also were collected during earlier visits to mines with deposits of interest. The aim was to obtain a uniform sample dataset analyzed as one batch using the best analytical procedures, thus avoiding comparisons between different data sources representing a variety of analytical techniques, variable detection limits, and incomplete analyses. The volcanic facies was taken into consideration when selecting samples. For example, in lobed felsic volcanic domes and flows, only the lobe center or the massive facies was sampled to reduce the possible influence of hydrothermal alteration. The goal of the sampling strategy was to compare (1) VMS-hosting rhyolites to surrounding rhyolites, (2) rhyolites from different mining districts, and (3) rhyolites from areas considered relatively nonprospective for VMS deposits to rhyolites from known VMS districts. A special emphasis was given to rhyolites associated with documented atypical (vein and disseminated) gold-rich volcanogenic deposits (e.g., Géant Dormant, Comtois, Agnico-Telbel, Duvan). Furthermore, dated rhyolites and felsic tuffs were also sampled to provide a temporal framework for the evolution of the felsic volcanism.

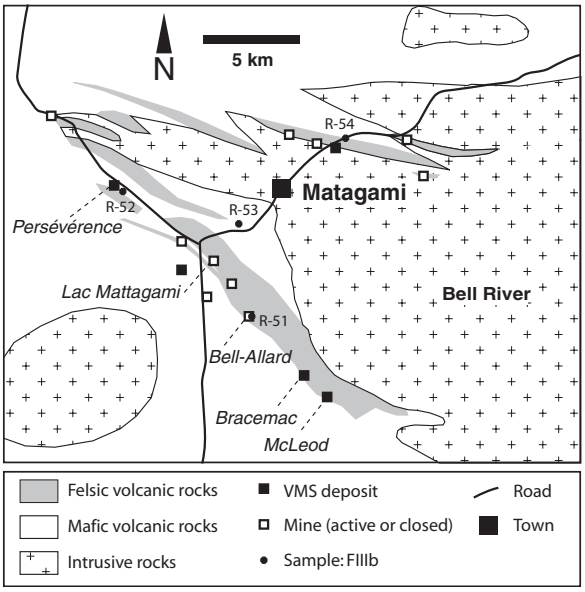

FIG. 2. Simplified geologic map of the Matagami district, showing sample and VMS deposit locations. Map modified from Piché et al. (1993).

Geochemical analysis

All samples were processed at the Université du Québec à Chicoutimi where they were cleaned to remove surface weathering, crushed, and then pulverized using an alumina shatter box. The shatter box was cleaned with quartz between each sample and precontaminated with each new sample to minimize sample-to-sample contamination. The powdered samples were shipped to the Geo Labs facility in Sudbury as one batch. The major elements were analyzed using wavelength-dispersive X-Ray florescence (WXRF) on fused pellets.

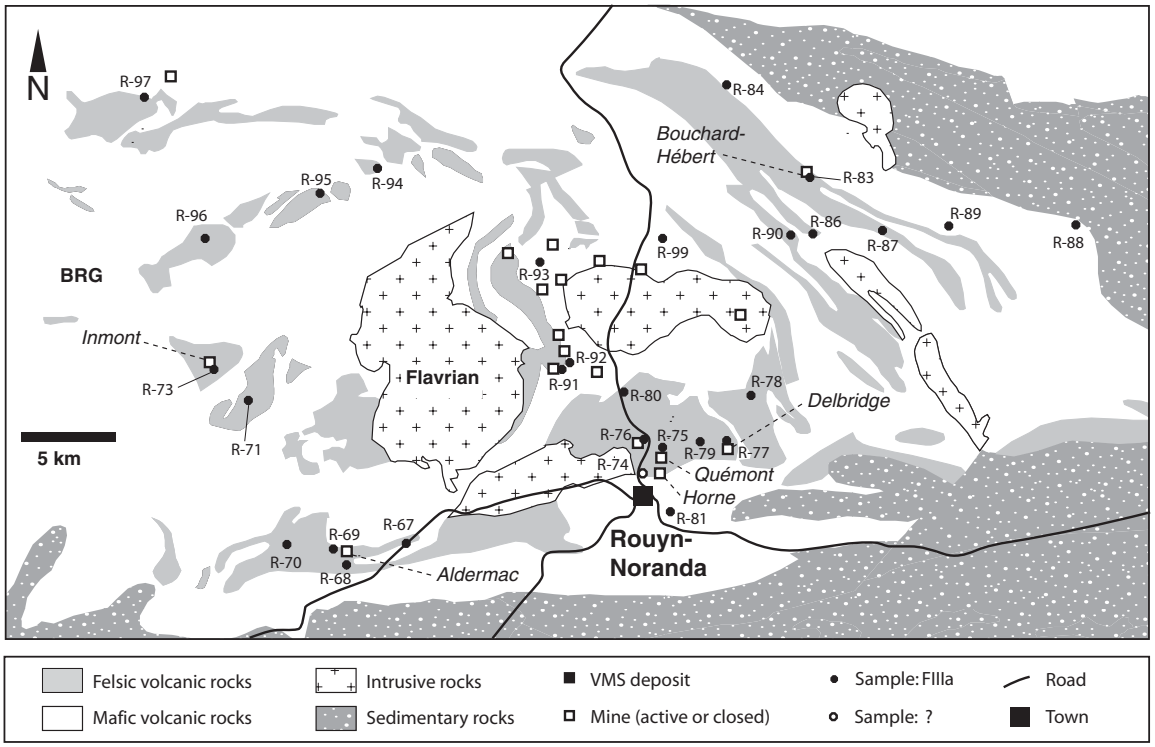

FIG. 3. Simplified geologic map of the Noranda district, showing sample and VMS deposit locations. BRG = Blake River Group. Map modified from Pearson and Daigneault (2009).

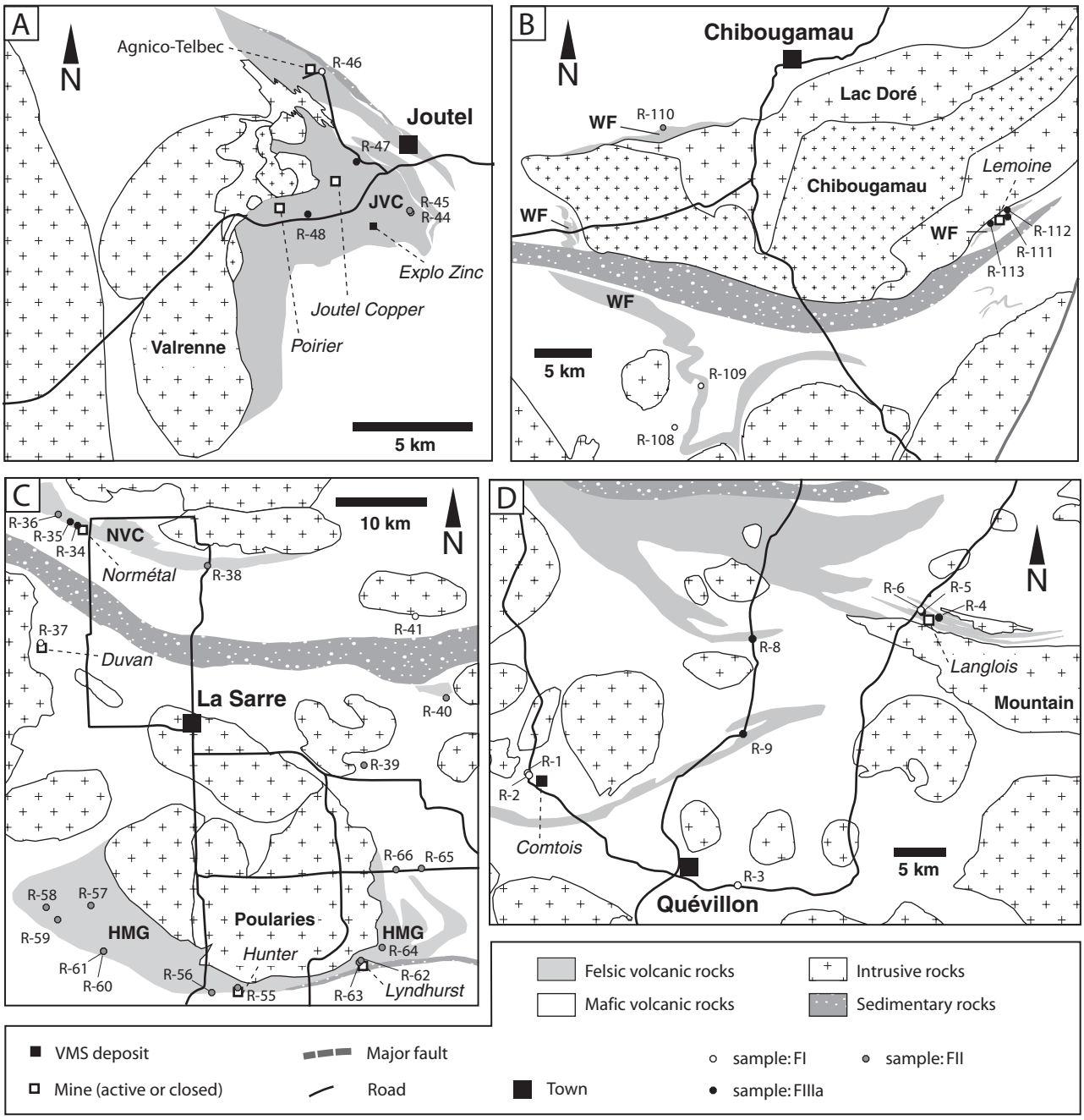

FIG. 4. Simplified geologic map, showing sample and VMS deposit locations. A. Joutel (modified from Legault et al., 2002). JVC = Joutel Volcanic Complex. B. Chibougamau (modified from Daigneault and Allard, 1990). WF = Waconichi Formation. C. Normétal (upper part: modified from Lafrance et al., 2000) and Hunter (lower part: modified from Mueller and Donaldson (1992). HMG = Hunter Mine Group, NVC = Normétal Volcanic Complex. D. Quévillon area (modified from Lacroix et al., 1993).

Trace elements were determined by ICP-MS following a closed-beaker digestion method involving four acids over two weeks to ensure total digestion of all minerals. Three replicates and one reference sample were included in the batch. The precision and accuracy of the analytical values were excellent, including the results for potentially problematic Zr (standard deviation of <0.05% for trace elements). The analytical results used in this study are provided in Appendix 1.

Petrographic study

Thin sections were made from all samples except for those from drill core and samples of insufficient size (App. 2). The goal of the petrographic study was to establish, (1) the percentage and size of phenocrysts, (2) the nature of any of feldspar phenocryst alteration, and (3) the mineral assemblage, overall composition, and intensity of the quartz-feldspar matrix alteration.

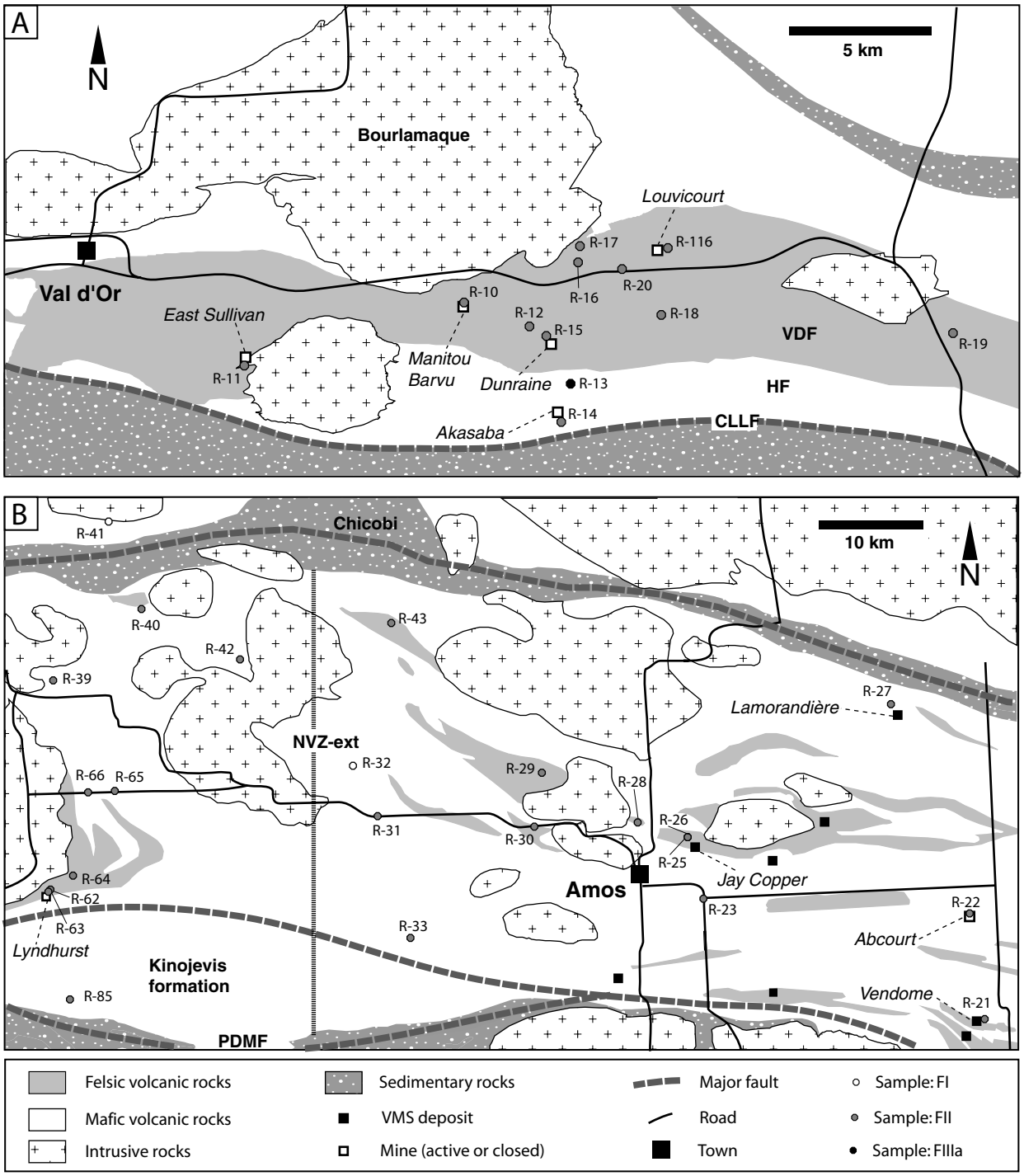

FIG. 5. A. Simplified geologic map, showing sample and VMS deposit locations. B. Val-d'Or district (modified from Scott et al., 2002). CLLF = Cadillac-Larder Lake fault, HF = Heva Formation, VDF = Val-d'Or Formation. B. External North Volcanic zone (NVZ) area (modified from Chown et al., 1992). PDMF = Porcupine-Destor-Manneville fault.

Assessment of Rhyolite Type Versus VMS Potential

Assessing exploration vectors and prospectiveness indicators based on the presence of mineralization, number of deposits, and total ore tonnage is limited by the current state of knowledge and assumes that discovered orebodies represent high potential, and undiscovered mineralization represents low potential. Sampling bias is another limiting constraint because it is difficult to obtain a uniform sampling pattern. The VMS districts, particularly the best studied ones, are invariably oversampled, whereas smaller or remote districts are commonly underrepresented, as are other areas considered to have low potential. Although it is impossible to overcome all these limitations, this study has the advantage of including a wide range of felsic volcanic rocks, whether associated with VMS mineralization or not.

In the following sections, mining districts and areas of interest are described and classified in terms of predominant rhyolite-VMS associations, with rhyolite types determined according to parameters of Hart et al. (2004). Although our approach uses informal subdivisions of mining districts, effusive centers, and geographic sectors that may have multiple felsic horizons, and in some cases, various rhyolite types, it has numerous advantages described above.

The geochemical signatures of rhyolites directly associated with VMS and VMS-related mineralization are compared to other rhyolites from the same district, referred to here as "background rhyolites," in an attempt to uncover any geochemical trends within districts. Tonnage values for the various districts were compiled using data from Chartrand and Cattalani (1990), Lacroix (1998), and Hannington et al. (1999a), in addition to data from companies where necessary. Ore, alteration, and volcanic host-rock characteristics were also compared (Tables 1, 2).

To overcome the effect of hydrothermal alteration in classifying the rhyolite samples, only HFSE and REE were used. Some altered rhyolite (or dacite) samples in the footwall and lateral to VMS deposits have major element concentrations ranging from apparent andesite (<63%) to high-silica rhyolite (>80% SiO_2). Even trace elements (LREE) reputed to be immobile show some variations in strongly altered footwall rocks and these particular samples are identified in the text. It should be noted, however, that with the exception of these anomalous altered rhyolites, most samples display no differences in REE and HFSE concentrations compared to the background rhyolites and are thus considered suitable for the purpose of this study.

Rhyolite Classification and Petrogenesis

Four types of rhyolite are identified by Lesher et al. (1986): FI, FII, FIIIa, and FIIIb. The FIV-type rhyolites (Hart et al., 2004) are virtually absent from Archean suites and are not discussed. The FI rhyolites are alkaline to calc-alkaline, with strongly fractionated REE patterns and strongly negative Ta and Nb anomalies. They are considered barren to rarely favorable for hosting VMS deposits. The FII rhyolites are calc-alkaline to transitional (following the nomenclature of Barrett and MacLean, 1994), with moderately fractionated REE patterns and moderate Ta and Nb anomalies. They are considered moderately favorable for hosting VMS deposits. The FIIIa and FIIIb rhyolites are tholeiitic and considered to have the greatest potential for hosting VMS deposits. The FIIIa rhyolites show weakly fractionated REE patterns and weak to nonexistent Nb and Ta anomalies. The FIIIb rhyolites are high-temperature rhyolites with flat REE patterns that lack Ta and Nb anomalies.

Recently, Hart et al. (2004) linked the geochemical signatures of various rhyolite types to partial melting depths within a rift environment. The FI, FII, and FIII magmas are interpreted as having equilibrated with garnet-bearing residua at a depth of >30 km, with amphibole-plagioclase residua at 30 to 10 km, and with plagioclase-dominant, garnet-amphibole–free residua at <15-km depth, respectively.

Hart et al. (2004) provided a list of compositional ranges to discriminate between the four rhyolite types. Four of the most useful elements are Zr, Y, La, and Yb because they are generally immobile during hydrothermal alteration and are representative of petrogenetic processes. These elements were used to create Zr/Y versus Y and $[La/Yb]_{CN}$ versus Yb_{CN} (chondrite-normalized: Nakamura, 1974) binary classification diagrams (Lesher et al., 1986; Barrie et al., 1993; Lentz, 1998). A drawback of these classification parameters is the overlap of some discriminating compositional ranges for the various rhyolite types. When plotted on the binary diagrams (Fig. 6), only 61 percent of the samples fall into the same classification field on both plots. To overcome this discrepancy, primitive mantle-normalized multielement plots were used in this study. These plots allow for better discrimination between rhyolite signatures, and distinguishing features, such as negative Nb and Ta anomalies associated with subduction processes, Eu anomalies, and degree of REE fractionation, can be better visualized (e.g., Sun and McDonough, 1989; Kerrich and Wyman, 1997).

FIIIb Rhyolites

The FIIIb rhyolites are defined as tholeiitic high-silica, high-temperature rhyolites with flat rare earth element (REE) patterns expressed by $[La/Yb]_{CN}$ chondrite-normalized values of 1.1 to 4.9, high concentrations of high field strength elements (Y, Zr, Hf, and HREE), low Zr/Y ratios, pronounced negative Eu anomalies, and a lack of subduction-related anomalies such as Nb and Ta (Hart et al., 2004). This type of rhyolite was initially identified at Kidd Creek, Kamiskotia, and in the Matagami district (Lesher et al., 1986).

Matagami mining district

The Matagami area (Fig. 2) is an important VMS district with total past production and current reserves of more than 50 Mt of ore from 12 deposits, including the 5-Mt Zn-Cu Perseverance deposit presently under development (Xstrata Zinc). The volcanic succession is folded along the open northwest-plunging Galinée anticline (Sharpe, 1968), which is centered on the synvolcanic Bell River intrusion. The south flank is a low-strain domain with the volcanic sequence facing and dipping 45° south, whereas the north flank is a highly strained, steeply dipping domain (Piché et al., 1993). The stratigraphic succession comprises the 2721 Ma (Mortensen et al., 1993) rhyolitic Watson Lake Group at the base overlain by the basaltic Wabasse Group (Beaudry and Gaucher, 1986). The Watson Group consists of a 1,000-m-thick sequence of felsic lava flows representing the footwall of VMS deposits in the region, with the exception of the newly discovered Bracemac and McLeod deposits. All the deposits, except Bracemac and McLeod, lie along a cherty and sulfide-enriched unit called the Key tuffite at the interface of both groups (Piché et al., 1993).

The south and north flanks of the Watson Group were sampled from: (1) the underground footwall at the Bell-Allard mine, (2) a surface stripping of the rhyolite hosting the Perseverance deposit, (3) the location of the rhyolite for which Mortensen et al. (1993) determined a geochron U-Pb age of 2721 Ma (sample R-53 in this study), and (4) rhyolites north of the town (Fig. 2). All four samples have flat HFSE-REE patterns as previously documented by Lesher et al. (1986) and Barrie et al. (1993), and the pattern for the Bell-Allard footwall rhyolite sample is the same as the pattern for the other three (Fig. 7).

TABLE 1. Characteristics of Host Volcanic Sequences in Selected VMS Districts

Area	Group	Volcanic style	Vesicularity	Volcanic hiatus	Felsic composition evolution	Intrusion	Reference
Matagami	FIIIb	Bimodal mafic-felsic, lobate felsic lava flows with multicentered coalescent volcanism forming a unit of regional extent, well-documented synvolcanic faults	Low-medium	Key tuffite: main horizon hosting all deposits	Homogeneous at the district scale	Bell River	Piché et al. (1993)
Noranda	FIIIa	Bimodal mafic-felsic volcanism with multiple isolated to locally coalescent felsic centers, dominated by lobate felsic lava flows; well-documented synvolcanic faults, some of regional extent	Low	Multiple chert horizons defining multiple volcanic cycles	Homogenous at the district scale	Clericy Flavrian Powell	Kerr and Gibson (1993)
Joutel	FIIIa	Bimodal volcanism dominated by lobate felsic lavas with lesser tuffaceous rocks	Low	Cherty horizons (not well-delineated regionally)	Evolution from tholeiitic to transitional to calc-alkaline	Valrenne	Legault et al. (2002)
Normétal	FIIIa	Rift-related bimodal volcanism dominated by flows and lesser clastic facies; isolated felsic centers along synvolcanic faults bordering rift margins	Low	Banded iron formation at the top of the host unit	Evolution from transitional to tholeiitic	Unknown	Lafrance et al. (2000)
Quévillon	FIIIa	Strongly deformed bimodal sequences with poorly preserved volcanic facies and architecture	Low to none	Not documented	Variable at the district scale, numerous felsic horizons	Mountain	Lacroix et al. (1993)
Val-d'Or	FII	Andesite to rhyolite, volcaniclastic-dominated volcanism with local domes and lava flows proximal to effusive center; multicentered coalescent volcanism	High	Local fine-grained sediments	Similar at the district scale	Bourlamaque	Scott et al. (2002)
Selbaie	FII	Andesite to rhyolite, volcaniclastic-dominated volcanism with local dome and lava flows proximal to effusive center; multicentered coalescent volcanism	High	Local pyrite-rich sediments	Similar at the district scale	Brouillan	Larsen and Hutchinson (1993)
Hunter	FII	Caldera-related bimodal sequence, abundant felsic flows, large discordant felsic dike swarm	Low to none	Banded iron formation at the top of the host units	Similar at the district scale	Poularies	Mueller and Mortensen (2002)
Bousquet	FI and FII	Andesite to rhyodacite, volcaniclastic-dominated volcanism with local dome and lava flows proximal to effusive centers; multicentered coalescent volcanism	High	None	Similar at the district scale	Mooshla	Lafrance et al. (2003)

TABLE 2. Characteristics of VMS Deposits in Selected Districts

Areas	Group	Main deposits	Metals	Mineralization style	Alteration	Reference
Matagami	FIIIb	Mattagami Lake Bell-Allard Perseverance	Zn-Cu-Ag	Massive stratiform exhalative sulfide lenses above a regional cherty horizon with well-defined underlying discordant stringer zones	Chlorite Talc Sericite	Lavallière (1995)
Noranda	FIIIa	Quémont Ansil Corbet	Cu-Zn-Au-Ag	Massive stratiform exhalative sulfide lenses above regional cherty horizons with well-defined underlying discordant stringer and alteration zones	Chlorite Sericite	Kerr and Gibson (1993)
Noranda	FIIIa FII	Horne	Cu-Au	Cigar-shaped massive sulfide lenses replacing felsic volcaniclastic rocks with associated sulfide stringer zones (H zones); sulfide dissemination and replacement of felsic volcaniclastic rocks (Zn-rich zone 5)	Sericite Silicification ± Chlorite	MacLean and Hoy (1991)
Joutel	FIIIa	Poirier Joutel Copper	Zn- Cu-Ag	Folded massive sulfide lenses with bedded pyrite hosted in massive to brecciated and cherty rhyolite with associated discordant Cu-rich stringer zones in chloritic alteration	Chlorite Sericite Silicification	Legault et al. (2002)
Normétal	FIIIa	Normétal Normetmar	Zn-Cu-Au-Ag	Strongly deformed, vertically plunging, cigar-shaped sulfide lenses	Chlorite Sericite Fe-carbonate	Lafrance (2003)
Quévillon	FIIIa	Langlois Zone 97	Zn-Cu-Au-Ag	Strongly deformed and transposed as vertical tabular sulfide lenses; very weak preservation of original volcanic characteristics	Chlorite Sericite	Lacroix et al. (1993)
Val-d'Or	FII	Louvicourt East Sullivan Manitou-Barvue	Cu-Zn, Au-Ag	Mostly disseminated sulfides and associated massive replacement-type pods and lenses; no recognized well-defined discordant stringer zone or chert; mineralization occurs at various stratigraphic levels at the district scale	Chlorite Sericite Fe-carbonate	Jenkins and Brown (1999)
Selbaie	FII	Zone A1, A2, B	Cu-Zn-Au-Ag	Massive sulfide Cu- and Au-rich discordant lenses (A2 and B), disseminated and stringer Zn-rich sulfide mineralization in felsic volcaniclastic rocks, massive concordant pyritic lenses of low grade (A1)	Chlorite Sericite Silicification	Larsen and Hutchinson (1993)
Hunter	FII	Hunter Lyndhurst	Cu-Zn-Au-Ag	Concordant, exhalative massive sulfide lenses with underlying discordant stringer zones; deposits are at the top of the volcanic pile near iron formations and sediments	Chlorite Sericite	Bonneau (1992)
Bousquet	FI and FII	Laronde Bousquet 1 and 2 Dumagami	Au-Cu-Zn-Ag Au-Cu	Replacement-type gold-rich sulfide lenses in volcaniclastic horizons, no associated chert, no discordant stringer zone; mineralization occurs at various stratigraphic levels at the district scale	Aluminous Chlorite Sericite	Mercier-Langevin (2005)
Joutel	FI	Agnico-Telbel	Au-Ag	Disseminated to massive bands of gold-bearing pyrite	Fe-carbonate Chlorite Sericite	Gauthier et al. (2003)
Quévillon	FI	Comtois	Au-Ag	Disseminated to stringer-style gold-bearing pyritic mineralization	Aluminous	Dupré et al. (2002)
NVZ-int[1]	FI	Géant Dormant	Au-Ag (Cu, Zn)	Variably oriented sulfide-rich quartz veins	Chlorite Sericite	Gaboury and Daigneault (1999)
NVZ-ext[1]	FI	Duvan	Cu-Ag	Disseminated to massive bands of pyrite with abundant magnetite hosted in tuffaceous volcaniclastic rocks	Chlorite Sericite	Tremblay et al. (1996)

[1] Abbreviations: NVZ-ext = external North Volcanic zone, NVZ-int = internal North Volcanic zone

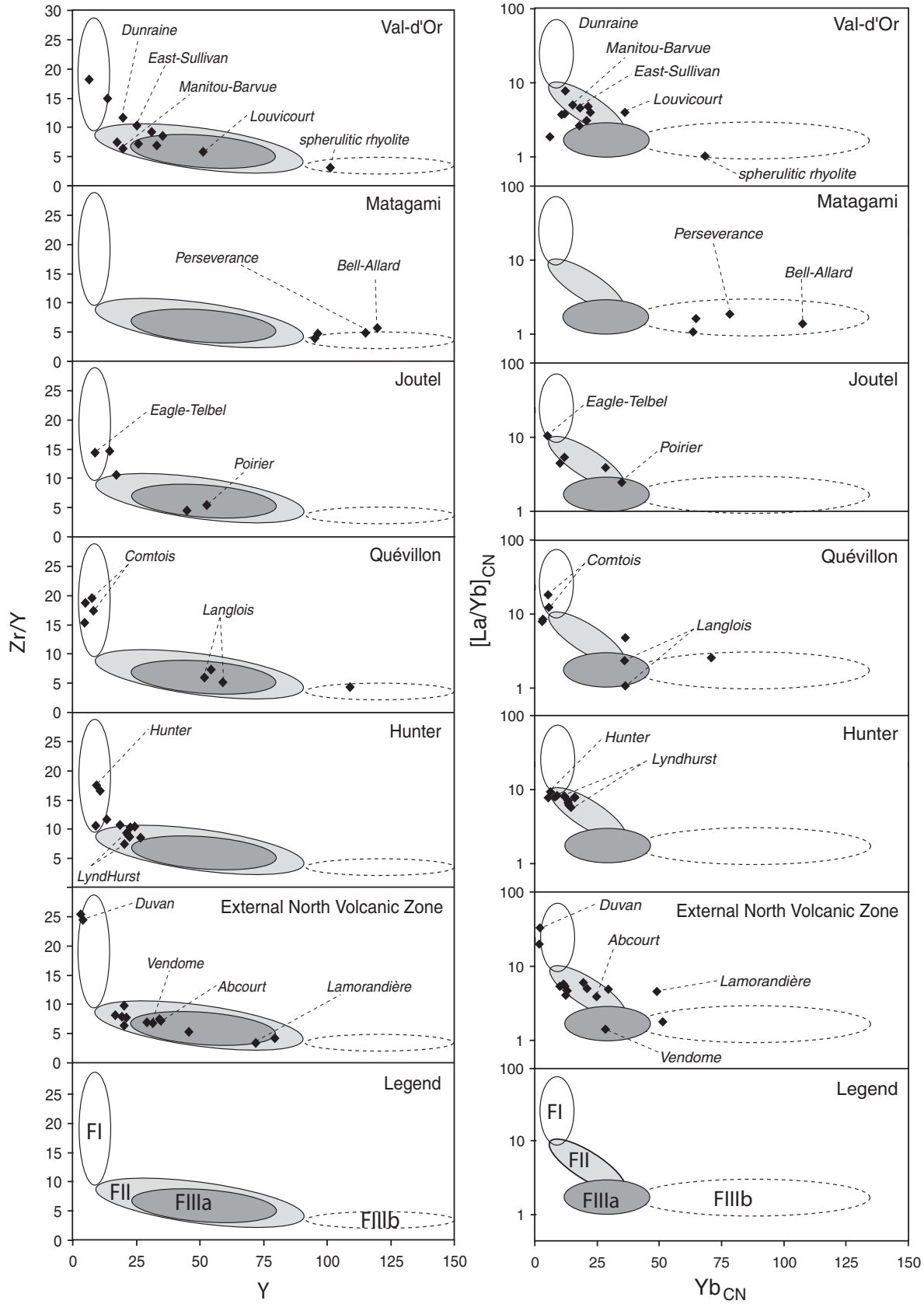

FIG. 6. Binary classification diagrams of Zr/Y vs. Y (Lesher et al., 1986) and $[La/Yb]_{CN}$ vs. Yb_{CN} (Barrie et al., 1993), showing some overlapping of discrimination fields leading to uncertainty in rhyolite classification. Classification fields are from Lentz (1998) and chondrite-normalizing values (CN) from Nakamura (1974).

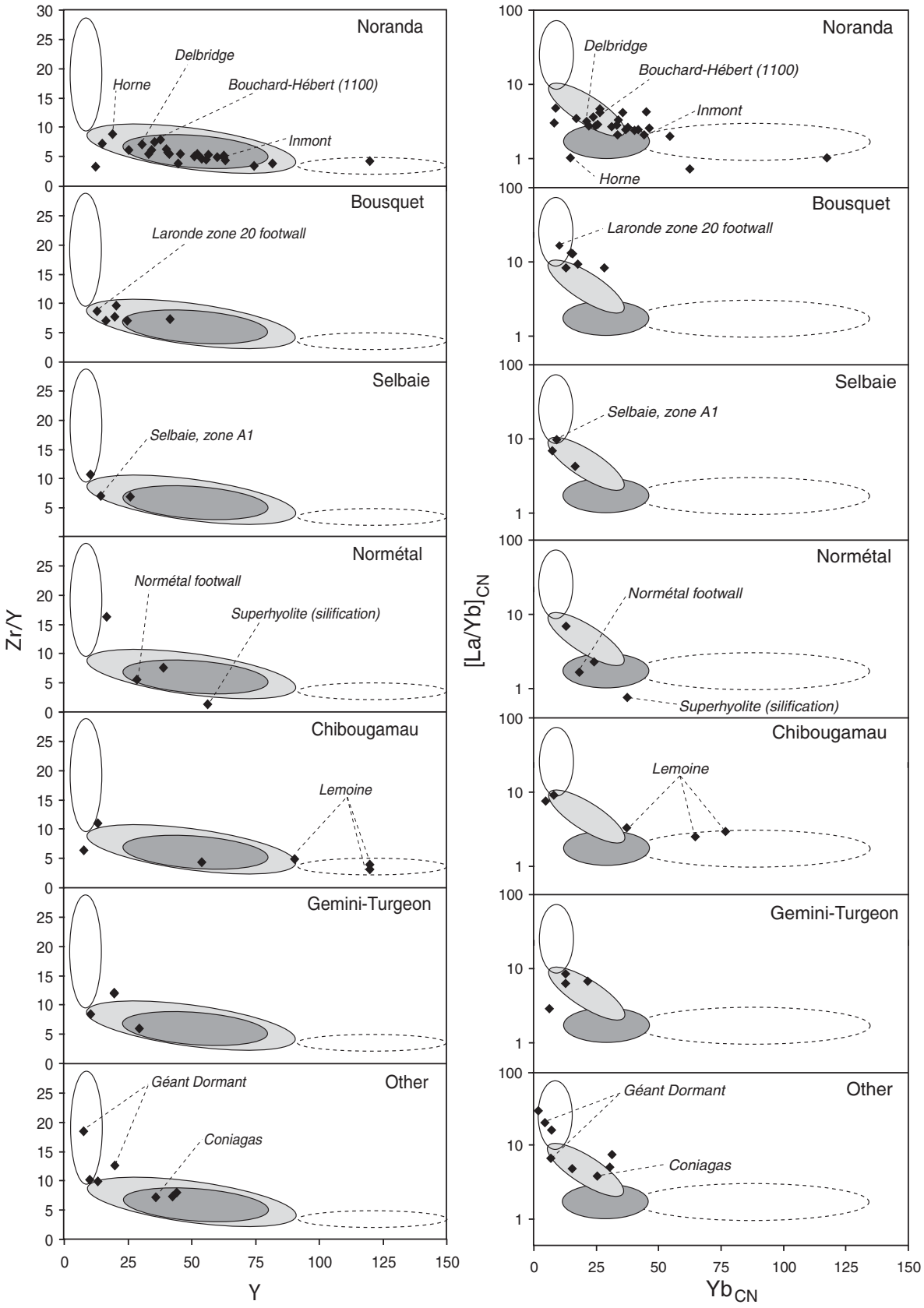
Noranda
Delbridge
Horne
Bouchard-Hébert (1100)
Inmont
Bousquet
Laronde zone 20 footwall
Selbaie
Selbaie, zone A1
Normétal
Normétal footwall
Superhyolite (silification)
Chibougamau
Lemoine
Gemini-Turgeon
Other
Géant Dormant
Coniagas
Zr/Y
Y
[La/Yb]CN
YbCN

FIG. 6. *(Cont.)*

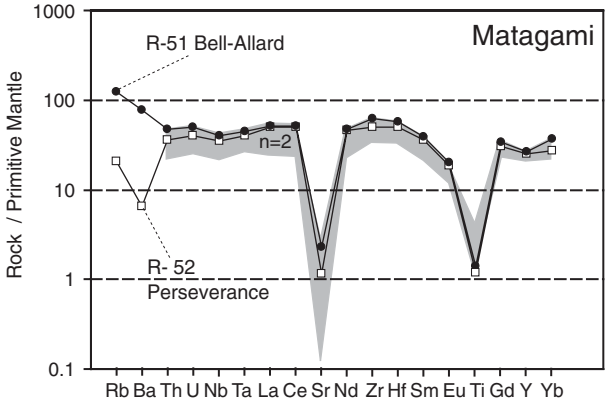

FIG. 7. Multielement plot normalized to primitive mantle (Sun and McDonough, 1989) for FIIIb felsic volcanic samples from the Matagami district. Gray envelope includes samples R-53 and R-54. The values for Rb and Sr are not included in the shaded pattern due to their mobility.

FIIIa Rhyolites

The FIIIa rhyolites are also considered to be tholeiitic, high-silica, high-temperature rhyolites, but they have slightly fractionated REE patterns with $[La/Yb]_{CN}$ chondrite-normalized values ranging from 1.5 to 3.5, low Zr/Y ratios, moderate HFSE contents relative to the primitive mantle, variable negative Eu anomalies, and weak, subduction-related negative Nb and Ta anomalies. This type of rhyolite was first described in the Noranda mining district (Lesler et al. 1986). Similar rhyolites have been identified in association with VMS deposits in the Joutel, Chibougamau, Normétal, and Quévillon mining districts.

Noranda

The Noranda mining district, located in the Blake River Group of the Southern Volcanic zone, is well known for its VMS deposits. More than 33 deposits totaling 135 Mt have been mined, including the world-class, gold-rich Horne mine (54 Mt). The 2706 to 2696 Ma (Pearson and Daigneault, 2009) Blake River Group comprises almost half of the Southern Volcanic zone, where it is considered to form a thick (up to 10–15 km) and laterally extensive stratovolcano covering an area of about 3,000 km^2 (e.g., Pearson and Daigneault, 2009). The volcanic stratigraphy consists of a bimodal sequence of rhyolite and andesite flows (Dimroth et al., 1982). Five volcanic cycles were defined near the synvolcanic Flavrian pluton (Gibson, 1990). Cycle 3 hosts a number of felsic units, some of which are separated by chert horizons that constitute the locus for VMS deposits (Gibson and Watkinson, 1990). The Blake River Group differs from most other parts of the Abitibi belt by its exceptional state of preservation, with only weak deformation and subgreenschist facies metamorphism, and it has been the focus of numerous geochemical studies (e.g., Gélinas et al., 1984; Peloquin et al., 1996).

Twenty-two samples were collected across the Blake River Group (Fig. 3). The strategy was to collect samples within and around the footwall of VMS deposits and away from known VMS deposits, and to cover most accessible and exposed rhyolite horizons. Samples from the Bouchard-Hébert and Inmont mines are from the immediate footwall. Samples from the Horne and Delbridge mines are from lateral extensions of the host rhyolite. Figure 8A shows that 20 of the samples have the characteristics of FIIIa rhyolites. Sample R-92 has lower mantle-normalized element abundances but a similar HFSE-REE pattern (except for Ti), whereas REE fractionation is more pronounced in sample R-90. Samples from the VMS deposits plot within the range of background rhyolite compositions (shaded area in Fig. 8B), except samples R-74 and R-82. Sample R-74 from the Horne mine shows weak to intermediate REE depletion. Intense hydrothermal alteration, as indicated by strong sericitization in thin section (App. 2), likely explains the depletion of REE. MacLean and Hoy (1991) documented similar LREE mobility caused by intense hydrothermal alteration of rhyolite at the Horne mine. However, the lower abundances of the more immobile elements, such as Y and Yb, suggest an underlying more fractionated initial REE signature, a feature also documented by MacLean and Hoy (1991) at the Horne mine. These findings are consistent with those of Peloquin et al. (1996).

Joutel

The Joutel volcanic complex is 5 to 7 km thick and consists of bimodal basalt-rhyolite successions that formed during five episodes of volcanism, which evolved from tholeiitic to transitional to calc-alkaline (Legault et al., 2002). Phase 2 (2728 ± 2 Ma: Mortensen et al., 1993) is a 2- to 3-km-thick sequence composed mostly of dacite and rhyolite flows hosting three Zn-Cu-Ag VMS deposits, the Poirier (7 Mt), Joutel Copper (1.7 Mt), and Explo-Zinc (1 Mt) deposits (Fig. 4A). A limited number of geochemical analyses were performed on rocks from the major VMS-hosting unit. Phase 5 is represented by a 100- to 300-m-thick and laterally extensive (20 km) tuffaceous felsic calc-alkaline unit that hosts the volcanogenic Eagle-Telbel Au-Ag massive to semimassive sulfide deposit (Gauthier et al., 2003). These rocks are interpreted to be FI type (see below).

We collected samples from a rhyolite unit with U-Pb zircon ages of 2728 Ma (Mortensen et al., 1993: sample R-47), near known VMS deposits, and at locations some distance from the VMS deposits (Fig. 4A). The felsic tuff hosting the Eagle-Telbel Au-Ag deposit was also sampled. Two types of rhyolites, FII and FIIIa, were found (Fig. 8C). The FIIIa rhyolites are spatially associated with the Poirier and Joutel VMS deposits, whereas FII rhyolites are located at the top (eastern part) of the Joutel volcanic complex.

Chibougamau (Lemoine)

The Chibougamau area is known for its epigenetic Cu-Au sulfide veins (Pilote et al., 1998), rather than VMS-type deposits. One exception is the small (0.75 Mt) but very high-grade and gold-rich Cu-Zn-Au-Ag Lemoine deposit hosted by the felsic Waconichi Formation (Guha et al., 1988). This 2730 Ma (Mortensen et al., 1993) formation forms a thin, dominantly calc-alkaline belt that can be traced throughout the Chibougamau area (Fig. 4B). It is mainly tuffaceous in nature, with lesser porphyritic intrusions (Daigneault and Allard, 1990). Near the now-closed Lemoine mine, the felsic rocks are tholeiitic (Gobeil, 1980) and have well-defined, lobed lava flow facies indicating a proximal effusive center.

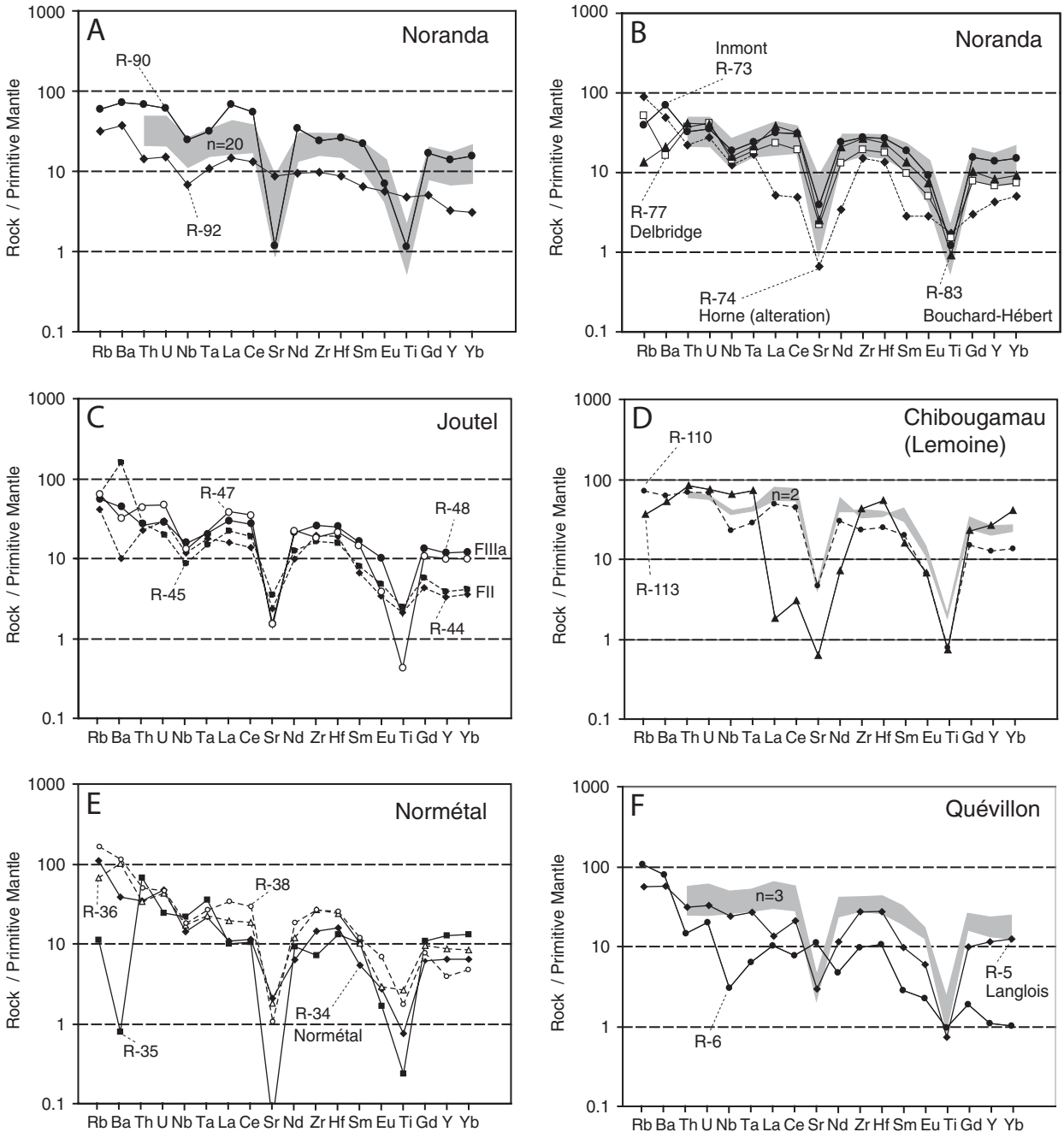

FIG. 8. Multielement plots normalized to primitive mantle (Sun and McDonough, 1989) for FIIIa felsic volcanic samples from various districts. A. Noranda district: gray envelope includes samples R-67 to -71, R-73, R-75 to -81, R-83, R-84, R-88, R-89, R-93, R-95 to -97, and R-99 away from VMS. B. Noranda district: plots of rhyolite samples directly associated with VMS deposits. C. Joutel district: dashed-line samples are FII rhyolites. D. Chibougamau area: gray envelope includes samples R-111 and R-112. E. Normétal district: dashed-line samples are FII rhyolites. F. Quévillon area: gray envelope includes samples R-4, R-8, and R-9.

Three samples were collected around the Lemoine deposit and three others from the Waconichi Formation away from the deposit (Fig. 4B). Samples from Lemoine have HFSE-REE patterns typical of FIIIa rhyolites (Fig. 8D). One strongly chloritized, silicified, and sericitized sample (R-113; App. 2) has lower LREE (La, Ce, Nd) contents presumably caused by intense hydrothermal alteration (Campbell et al., 1984; MacLean, 1988). Sample R-110 to the north has an FII signature, and samples R-109 and R-108, as previously noted, are FI tuffs (see sections on FI and FII rhyolites below). The various signatures from the extensive Waconichi Formation suggest a volcanic evolution or an unrecognized complexity including various volcanic vents of specific geochemical compositions.

Normétal

The 4-km-thick Normétal volcanic complex forms a southeast- to east-trending, steeply dipping, monoclinal volcanic succession that can be traced along strike for 35 km (Fig. 4C). It consists of basaltic andesite, dacite, and rhyolite erupted during five distinct volcanic phases with an intervening sedimentary phase (Lafrance et al., 2000; Mueller et al., 2008). Two VMS deposits were mined: the 11-Mt Cu-Zn-Au-Ag Normétal deposit and the smaller (0.2-Mt) Zn-rich Normetmar deposit. The associated volcanic center consists of a mafic-dominated shield volcano of transitional affinity which evolved to a felsic-dominated composite volcano with three principal vent sites of tholeiitic affinity dated at 2728 Ma (Mortensen et al., 1993). The VMS deposits are associated with the last stage of tholeiitic felsic volcanism.

Samples were collected along the felsic horizon, 2.5 km west (sample R-36) and 14 km east (sample R-38) of the Normétal deposit, and from its immediate vicinity (samples R-35, R-36: Fig. 4C). Rhyolites spatially associated with VMS mineralization are typically FIIIa (Fig. 8E), whereas samples away from the deposit have fractionated HFSE-REE patterns with characteristics comparable to FII-type rhyolites (see FII section).

Quévillon

The Quévillon area hosts the Zn-Cu-Ag Langlois mine (previously known as the Grevet mine) as well as other deposits that are currently being explored (e.g., the Orphee zone) or developed (e.g., the 97 zone of Breakwater Resources Ltd). This area has past production and reserves totaling more than 20 Mt of ore (Lacroix et al., 1993). The Grevet-Mountain volcanic complex, dated at 2718 Ma (Davis et al., 2005), is bound to the north by a tonalitic intrusion and to the south by the synvolcanic Mountain pluton (Fig. 4D). The volcanic setting of the deposits is poorly understood because the volcanic strata lie along a major southeast-trending regional discontinuity known as the Cameron fault (Lacroix et al., 1993). The favorable, steeply dipping, 2-km-thick volcanic sequence has been traced along strike for more than 20 km (Fig. 4D). Around the Langlois mine, felsic rocks alternate with mafic bands and are transposed by penetrative schistosity (Lacroix et al., 1993). Regionally, the Quévillon area consists of numerous southeast- to east-trending rhyolitic bands, some of which consist of lava flows and domes, and others of tuffaceous rocks (Fig. 4D). In addition to VMS mineralization, the Quévillon area hosts the Comtois gold deposit—an atypical, volcanogenic disseminated sulfide deposit (Dupré et al., 2002) associated with FI rhyolite (see below).

A rhyolite sample taken near the Langlois mine (Fig. 4D) has an FIIIa signature (sample R-4), and other FIIIa rhyolites were also found in the Quévillon area (samples R-8, R-9: Fig. 8F). Sample R-6, collected near the mine, has a more fractionated REE pattern and lower amounts of mantle-normalized values (Fig. 8F). This sample may represent an interbedded tuffaceous horizon within the FIIIa host sequence of the Langlois mine. The sample from the footwall of the Langlois mine (R-5) has lower mantle-normalized REE abundances relative to Ta, Zr, Hf, and Y. The high concentration of SiO_2 (86 wt %) indicates strong silicification, which is supported by the petrographic data (App. 2), and this likely accounts for the variability in REE concentrations. Other samples (R-1, R-2, and R-3) represent FI rhyolites and are discussed below.

FII Rhyolites

The FII rhyolites have calc-alkaline to transitional affinities, gently sloping REE patterns indicated by $[La/Yb]_{CN}$ chondrite-normalized values of 1.7 to 8.8, moderate Zr/Y ratios, intermediate HFSE concentrations, variable Eu anomalies, and moderately negative Ta and Nb anomalies. They are interpreted as arc-related rhyolites (Barrie et al., 1993; Hart et al., 2004). Rhyolites of the FII category host VMS deposits in the Val-d'Or and Selbaie mining districts, and make up the Hunter volcanic complex and the largest portions of the external North volcanic zone and Gemini-Turgeon areas.

Val-d'Or

The Val-d'Or mining district (Fig. 5A) may be best known for its gold deposits, but it is also a major VMS district with ore production and reserves in excess of 60 Mt from six Cu-Zn-Ag-Au deposits (Jenkins and Brown, 1999). The VMS deposits are hosted within the south-facing, steeply dipping, and laterally extensive (40 km long) Val-d'Or Formation, measuring 3 to 5 km thick (Pilote et al., 1999; Scott et al., 2002). This 2704 Ma formation comprises a complex subaqueous volcano-sedimentary sequence dominated by volcaniclastic deposits ranging from andesitic to felsic compositions, overlying the synvolcanic granodioritic Bourlamaque pluton (Scott et al., 2002). The VMS deposits are spatially associated with numerous, small, felsic-dominated volcanic centers of limited extent (Pilote et al., 1999). The volcanic rocks are mainly of transitional affinity and are interpreted as the products of arc volcanism (Scott et al., 2002). The 2701 Ma Heva Formation is 2 to 3 km thick, overlies the Val-d'Or Formation, and includes a laterally extensive, spherulitic dacitic unit that has been traced for 40 km along the base of the Heva Formation (Scott et al., 2002). The Heva Formation consists mainly of tholeiitic mafic rocks and is interpreted as a product of fissure-type volcanism (Scott et al., 2002). VMS deposits are not known in the Heva Formation, with the possible exception of the Akasaba Au-Ag deposit (Chartrand, 1989; Vovobiev, 2000).

The lithogeochemistry of felsic volcanic rocks from the Val-d'Or Formation was studied in detail by Pilote et al. (1999) and Scott et al. (2002). They concluded, using mainly Zr/Y ratios, that felsic volcanism evolved from tholeiitic to calc-alkaline near the top of the Val-d'Or Formation, although most units are of transitional affinity.

We collected samples underground from the footwall at the Louvicourt mine and at surface along the host rhyolite horizons at the former East Sullivan, Manitou-Barvue, and Dunraine mines (Fig. 5A). Samples were collected along a north-south transect within the Val-d'Or and Heva Formations and included the spherulitic dacitic unit and the eastern portion of the Sleepy volcanic center (Fig. 5A).

Multielement diagrams reveal that most rhyolite samples form a coherent group with typical FII characteristics (Fig. 9A). The spherulitic dacite sample (R-13) has an HFSE-REE pattern typical of FIIIa rhyolites (Fig. 9A). The low SiO_2 content (59.03%) suggests a more andesitic composition, but the

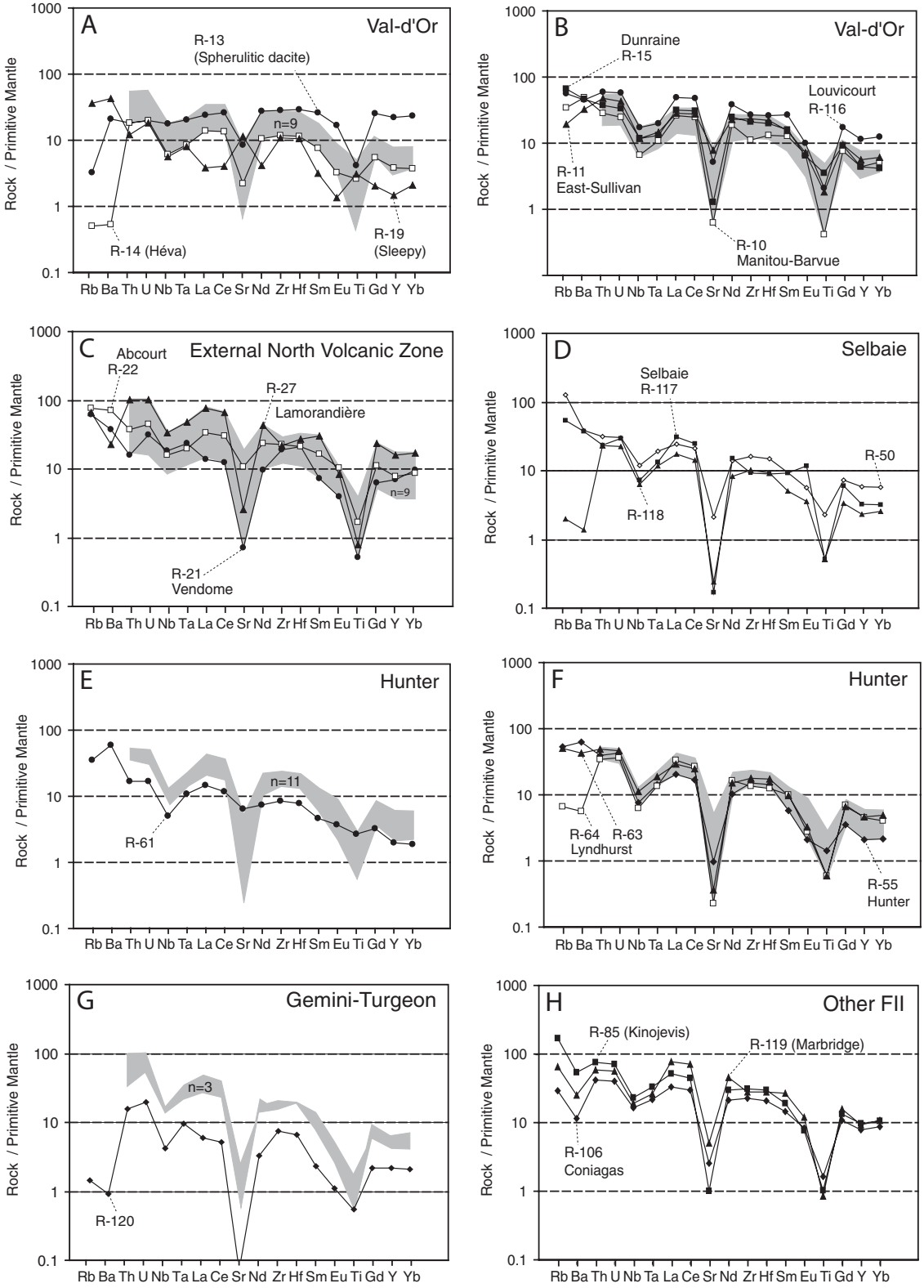

FIG. 9. Multielement plot normalized to primitive mantle (Sun and McDonough, 1989) for FII felsic volcanic samples from various districts. A. Val-d'Or district: gray envelope includes samples R-10 to R-12, R-15 to -18, R-20, and R-116 away from VMS. B. Val-d'Or district: plots of rhyolite samples directly associated with VMS deposits. C. External North Volcanic zone area: gray envelope includes samples R-23, R-25, R-26, R-28 to -31, R-42, and R-43. D. Selbaie district. E. Hunter district: gray envelope includes samples R-55 to -66, excluding R-61 away from VMS. F. Hunter district: plots of rhyolite samples directly associated with VMS deposits. G. Gemini-Turgeon area: gray envelope includes samples R-121 to -123. H. Other rhyolite samples with FII signatures.

unusual magnetite alteration observed in this sample (and in the unit generally) may account for the higher Fe_2O_3 and lower SiO_2 content of this dacitic rock (App. 1). The Sleepy sample (R-19) is characterized by an unusual signature, with La and Ce depletion relative to Zr and Hf, and lower HREE (Gd, Yb) and Y abundances compared to other samples. This signature may reflect hydrothermal alteration (La, Ce mobility) of a more fractionated rhyolite (lower HREE and Y). The presence of biotite (App. 2) suggests a higher metamorphic grade related to the proximity of the Grenville Province (Fig. 1) and also may account for the anomalous signature.

The tuff sample from the Heva Formation (R-14), dated at 2702 Ma (Pilote et al., 1999), has a HFSE-REE pattern similar to that of the rhyolite group, but with lower overall mantle-normalized values (Fig. 9A). The low Al_2O_3 content and LOI (App. 1) suggest that the sample is silicified, which would explain the lower HFSE-REE abundances. Samples taken near VMS deposits plot within the range of background rhyolites (shaded field, Fig. 9B), except for the Louvicourt footwall sample, which has the same REE-HFSE pattern but higher mantle-normalized element abundances.

External North Volcanic zone

The external North Volcanic zone covers a large area of about 6,000 km², spanning the towns of Lasarre, Amos, and Senneterre from east to west. It is bound by the linear Chicobi sedimentary unit to the north and by the Porcupine-Destor-Manneville fault to the south (Fig. 5B). This large area is dominated by mafic lavas with lesser bands of felsic volcanic rocks and local synvolcanic plutons (Gaboury, 2006). Ages range from 2727 to 2714 Ma (Labbé, 1999), indicating prolonged or multiphase volcanism. The large area is reputed to be a weakly favorable area for hosting VMS deposits. Except for the Abcourt deposit, only small VMS deposits have been discovered, including Jay Copper, Monpras, Trinity, Vendome 1 and 2, and Duvan (Fig. 5B). Although some deposits were explored underground (Amos, Duvan, Vendome), only the Abcourt deposit has been mined, producing about 6 Mt of ore grading 3 percent Zn and 40 g/t Ag (Labbé and Couture, 1999).

Fourteen samples of rhyolite were collected, four near the Abcourt, Duvan Vendome, and Lamorandière VMS deposits (Fig. 5B). Although the sampled area is large and contains rocks of various ages, the rhyolites define a coherent group of FII type in Figure 9C. Two represent FI-type rhyolites (R-37 at Duvan and R-32) and are discussed in the FI section below.

Selbaie mining district

The 2725 to 2730 Ma Brouillan Volcanic Complex (Barrie and Krogh, 1996) is mainly composed of felsic to intermediate calc-alkaline pyroclastic rocks forming an intracaldera sequence more than 1,200 m thick (Larsen and Hutchinson, 1993). The caldera sequence, which developed above the synvolcanic Brouillan tonalitic batholith, records an evolution from subaqueous to subaerial deposition. The south-facing volcanic sequence is tilted and may be traced laterally 12 km westward (Taner, 2000), but no significant deposit occurs away from the Selbaie mines. Selbaie is an atypical large-tonnage, low-grade volcanogenic Cu-Zn-Ag-Au deposit with both stratiform and epithermal characteristics that has yielded more than 50 Mt of ore (Larsen and Hutchinson, 1993). Mineralization occurs as veins and veinlets that cut the local stratigraphy at a high angle and as stratiform, massive to disseminated pyrite lenses of low metal content.

Barrie et al. (1993) concluded that rhyolitic rocks at Selbaie were of Group III in their classification system, which is equivalent to FII. For this study, two samples were collected from the open pit of the A1 mineralized zone and another from rhyolite 5 km west of the mine (Fig. 1). The multielement diagram indicates that these are of FII type with moderately fractionated REE and well-defined Ta-Nb anomalies typical of calc-alkaline rocks (Fig. 9D).

Hunter mine area

The 2728 to 2724 Ma Hunter mine group is a 6- to 7-km-thick volcanic sequence composed mainly of felsic lava flows and domes with lesser volcaniclastic felsic rocks, iron formations, and mafic pillowed and brecciated flows (Mueller and Mortensen, 2002). This group forms a 210-km² area of tilted, south-facing volcanic rocks overlying the synvolcanic, granodioritic Poularies intrusion (Fig. 4C). The main feature is a prominent north-trending felsic dike swarm, 5 to 7 km wide, interpreted as a caldera structure (Mueller and Donaldson, 1992; Mueller et al., 2008). To date, only two small Cu-Zn-Ag-Au VMS deposits have been discovered, Hunter and Lyndhurst, totaling less than 2 Mt of ore (Fig. 4C).

We collected 12 samples east and west of the Poularies intrusion (Fig. 4C). Included in this group are samples from the Hunter (R-55) and Lyndhurst mines (R-62, R-63), both past producers. Another sample, R-57, is from the north-trending felsic dike swarm. With the exception of R-61, which has lower mantle-normalized element abundances (Fig. 9E), the samples, including those from VMS deposits (Fig. 9F), define a coherent compositional group with a very restricted range of REE-HFSE mantle-normalized abundances typical of FII rhyolites. These results are consistent with those of Dostal and Mueller (1996) and demonstrate the very restricted chemical evolution of rhyolitic volcanism at the scale of the complex.

Gemini-Turgeon area

A felsic horizon with a thickness of about 2 km has been traced for more than 15 km in a north-south direction to the west of the synvolcanic Mistaouac pluton (Fig. 1). Rhyolites in this area are unexposed and all known geology has been deduced from drill core. The following description is from unpublished data of the IAMGOLD and Cancor mining companies and from Gobeil (2006). The volcanic units consist of a bimodal assemblage of porphyritic lava flows with few vesicles at the base, succeeded upward by predominantly felsic volcaniclastic rocks and a sedimentary sequence comprised of graywacke, siltstone, mudstone, and iron formations. U-Pb dating of zircons from the top of the volcanic pile yielded an age of 2735 Ma (Davis et al., 2005). Numerous small, massive, and disseminated volcanogenic sulfide lenses, with low Cu, Zn, Au, and Ag grades, occur mainly along the top of the volcanic sequence.

Four representative samples were provided by Cambior Inc. (now IAMGOLD) for this study. All samples are of FII-type rhyolite (Fig. 9G), although the $[La/Yb]_{MN}$ mantle-normalized values are among the highest of the FII-type rhyolites.

One sample (R-120), however, has lower REE-HFSE mantle-normalized abundances, probably caused by silicification (84.15 wt % SiO_2).

Other FII occurrences

Figure 9H shows a multielement diagram for other felsic rocks with FII signatures. Sample R-106 is from the mined-out 0.7-Mt Coniagas Zn-Pb-Ag VMS deposit (Fig. 1). Sample R-119 is a felsic tuff dated at 2718 Ma (Pilote et al., 1999), collected near the Marbridge Ni-Cu komatiite-hosted deposit (Fig. 1). Sample R-85 is from the 2718 Ma (Zhang et al., 1993) Kinojevis Formation (Fig. 5).

FI Rhyolites

The FI rhyolites are calc-alkaline, with strongly fractionated REE patterns, $[La/Yb]_{CN}$ chondrite-normalized values ranging from 5.8 to 34, low HFSE abundances, strong negative Ta and Nb anomalies, and variable Eu anomalies. They are interpreted as arc-related magmatic products (Barrie et al., 1993). These rhyolites occur in the Bousquet mining district and are spatially associated with other gold-rich volcanogenic deposits, namely the Géant Dormant (Sleeping Giant), Eagle-Telbel, and Comtois deposits, and the atypical Duvan Cu-Ag deposit.

Bousquet mining district

The Bousquet mining district is a world-class gold producer that includes Laronde—the world's largest polymetallic gold-rich VMS deposit (Mercier-Langevin et al., 2007a)—and pyritic gold-bearing replacement-type deposits such as Bousquet 1 and Dumagami-Bousquet 2 (Fig. 1). Total production and reserves amount to more than 100 Mt of ore. Recent regional studies have traced the 1.5- to 3-km-thick, south-facing, vertically tilted, strongly foliated, and east-trending volcanic Bousquet Formation for more than 20 km along strike (Lafrance et al., 2003). This 2696 to 2698 Ma Formation, which is part of the Blake River Group, consists of voluminous dacitic to rhyolitic vesicular volcaniclastic rocks with local felsic effusive lava flows and domes to which the VMS deposits are spatially associated (Lafrance et al., 2003). This sequence overlies the Mooshla synvolcanic tonalite-granodiorite pluton that hosts two synvolcanic, sulfide-rich vein-type gold deposits, Doyon and Mouska, both active producers. The Bousquet Formation is divided into lower and upper volcanic members. The lower member includes tholeiitic to transitional, mafic to felsic volcanic rocks, whereas the upper member is dominated by transitional to calc-alkaline, intermediate to felsic rocks (Lafrance et al., 2003; Mercier-Langevin et al., 2007a).

Sampling of the upper member was performed along a north-south section along Preissac Road, using the unit nomenclature of Lafrance et al. (2003). One sample (R-105) from the underground Laronde mine rhyolite (unit 5.3, which hosts the 20-N zone) was kindly provided by P. Mercier-Langevin (then of Agnico-Eagle) for this study. Overall, the samples display strong REE fractionation, the Laronde footwall sample having the strongest, and very pronounced negative Ta and Nb anomalies typical of FI rhyolites (Fig. 10A).

An exhaustive lithogeochemical study on the Laronde mine was recently conducted by Mercier-Langevin et al. (2007b). These authors interpreted some of the dacites and rhyolites of the upper member as belonging to the FI category, although they are dominated by FII-type rhyolites.

Other mineralized systems associated with FI rhyolites

Figure 10B shows a plot of mineralized felsic rocks with FI signatures from other locations, such as the Géant Dormant mine in the internal North Volcanic zone (Fig. 1), the Agnico-Telbel mine in the Joutel district (Fig. 4A), and the Comtois Au deposit in the Quévillon area (Fig. 4D). Mineralization styles range from sulfide-rich quartz veins (Géant Dormant: Gaboury and Daigneault, 1999) to sulfide disseminations in zones of highly altered rocks (Agnico-Telbel: Gauthier et al., 2003; Comtois: Dupré et al., 2002). All these deposits are hosted, at least in part, by felsic dikes and rhyolitic lavas of FI affinity (Géant Dormant, Comtois) or within FI-type felsic tuffs (Agnico-Telbel). The Cu-Ag Duvan mine is another example of atypical volcanogenic-related mineralization within FI felsic tuff. Mineralization occurs as concordant massive to disseminated pyrite and chalcopyrite associated with abundant magnetite (Tremblay et al., 1996).

Other FI occurrences

Numerous occurrences of tuffaceous rhyolite scattered across the Abitibi belt have FI signatures (Fig. 10C). They commonly occur as extensive regional units. Samples R-108 and R-109 are from the 2730 Ma (Mortensen et al., 1993) Waconichi Formation in the Chibougamau area (Fig. 4B), sample R-30 is from the Quévillon area (Fig. 4D), and two other samples (R-32, R-41) are from the North Volcanic zone (Fig. 5B). These units may be products of explosive eruption of felsic calc-alkaline magma with a high volatile content (e.g., Gibson et al., 1999). Other rhyolites from the Comtois (R-1) and Géant Dormant (R-115) deposits and the rhyolite (R-107) dated at 2791 Ma (Bandayera et al., 2004) are plotted in Figure 10D. The 2791 Ma rhyolite is unusually old relative to the 2735 to 2700 Ma ages for felsic volcanism in the Abitibi belt.

Discussion

The results of this study reveal that in small volcanic centers composed of various rhyolite types, such as Joutel, Chibougamau (Lemoine), Normétal, and Quévillon (Fig. 8), VMS deposits are specifically associated with FIIIa rhyolites. This demonstrates the usefulness of the approach for discriminating the most favorable sectors or horizons within small felsic volcanic centers. The much larger Noranda district is also characterized by rhyolites with FIIIa signatures, but the application of rhyolite chemistry in the exploration of this camp is less useful because FIIIa rhyolites are distributed over such a vast area (more than 3,000 km^2).

Regardless of rhyolite classification, there does not appear to be any link between ore tonnage and REE fractionation. VMS deposits are hosted by rhyolites with REE patterns ranging from low $[La/Yb]_{MN}$ mantle-normalized ratios or flat patterns (Matagami) to elevated $[La/Yb]_{MN}$ ratios or fractionated patterns (Bousquet-Laronde; Fig. 11). Furthermore, moderately fractionated FII rhyolites (Selbaie, Hunter, Vald'Or, and External North Volcanic zone) are variably mineralized, as was previously recognized by Lesher et al. (1986).

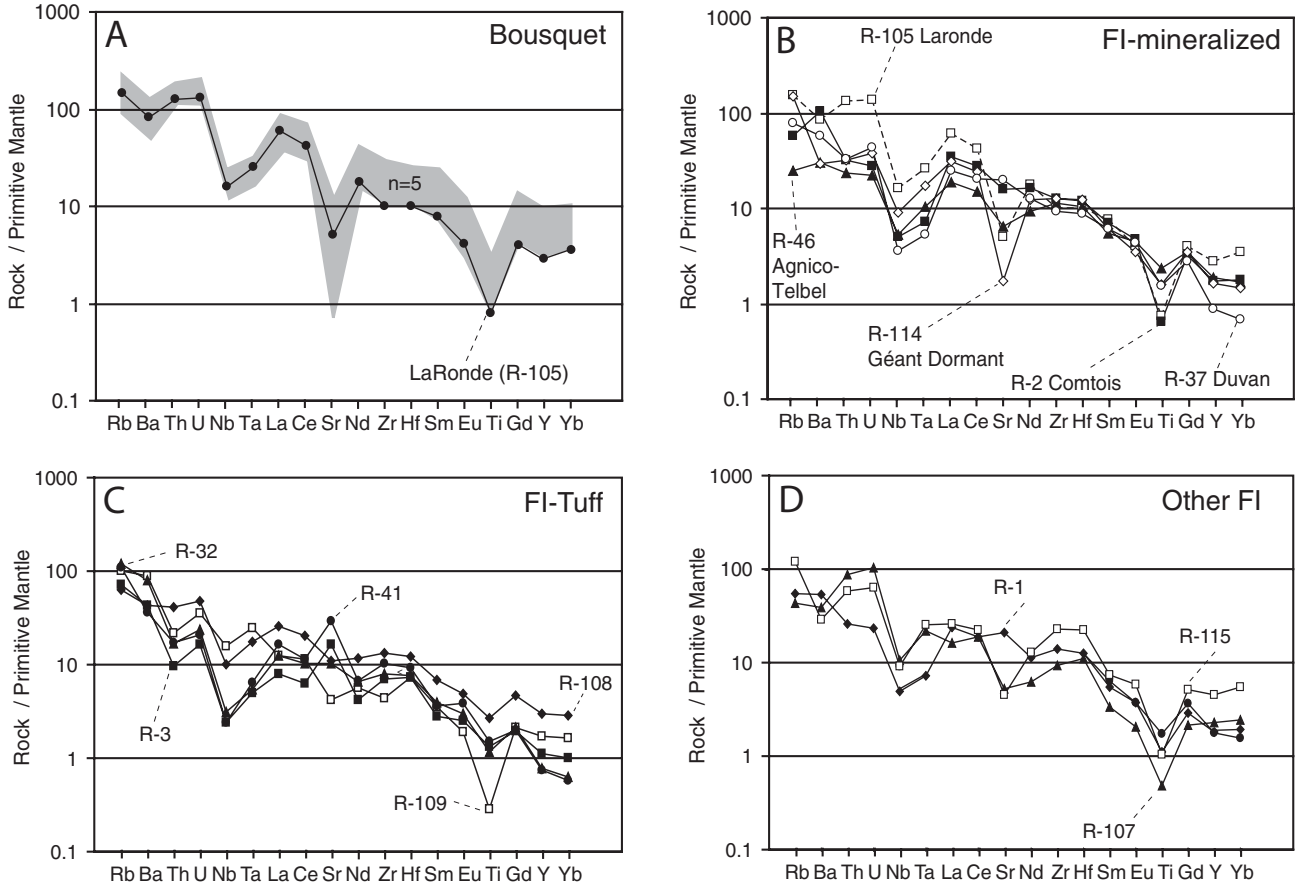

FIG. 10. Multielement plots normalized to primitive mantle (Sun and McDonough, 1989) for FI felsic volcanic samples. A. Samples from the Bousquet district. Gray envelope includes samples R-100 to -104. B. Mineralized samples from various locations. C. Samples from tuffaceous rhyolite at various locations. D. Other rhyolite samples with FI signatures.

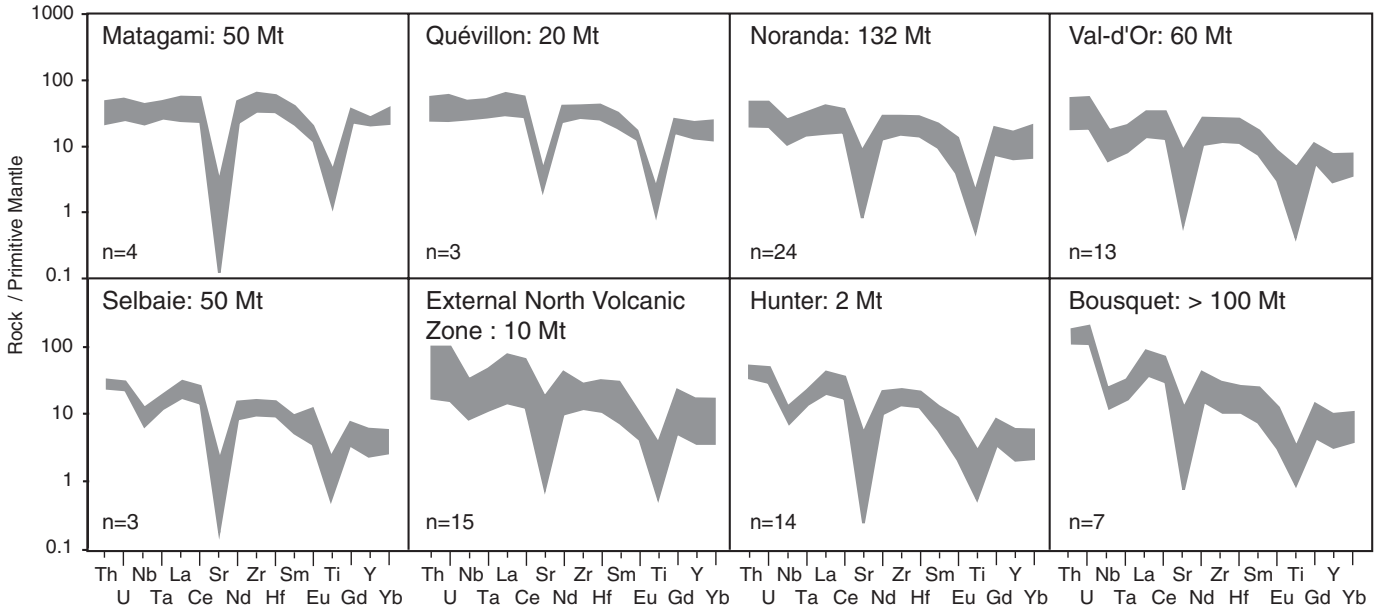

FIG. 11. Summary multielement plots normalized to primitive mantle (Sun and McDonough, 1989) for felsic volcanic rocks from mining districts, showing ore tonnages (production and reserve) in millions of metric tons (Mt).

Based on our dataset, it is not possible to attribute a greater VMS potential to specific rhyolite types based only on geochemical signatures.

Rhyolite petrogenesis and hydrothermal activity

The formation of VMS deposits is the product of convective hydrothermal activity induced by heat flux from an underlying magma chamber (Franklin et al., 1981, 2005). Fundamental factors that enable hydrothermal convection to occur include the structural permeability of the upper portion of the crust and the porosity of the volcanic pile (e.g., Morton and Franklin, 1987; Barrie and Hannington, 1999; Gibson et al., 1999; Davidson et al., 2004). Time is another key factor that is fundamental in maintaining the stability of the convective system and in accumulating sulfides on or near the sea floor (e.g., Barrie and Hannington, 1999; Franklin et al., 2005, and references therein).

Rhyolites are the result of petrogenetic processes involving partial melting, crystallization, fractionation, and assimilation (e.g., Hart et al., 2004). The depths at which these processes occur, the magma ascent rates, and the residence times in the crust also influence rhyolite chemistry. The same factors influence hydrothermal convection and VMS formation (e.g., in terms of thermal requirements). However, this study illustrates that different types of rhyolites are not necessarily more favorable than others to host VMS deposits. This may be because VMS formation is mainly related to processes that occur at shallow levels in the crust (<5 km: see Franklin et al., 2005) rather than at great depth (<30 km: see Hart et al., 2004) where the rhyolite magma is generated.

High-temperature FIII-type rhyolites (e.g., Noranda and Kidd Creek) have low amounts of phenocrysts and microphenocrysts (Hart et al., 2004). This generally aphyric texture is thought to reflect a rift setting where magma is rapidly transferred from the melt zone to the surface (Lentz, 1998; Hart et al., 2004) and quartz and feldspar do not accumulate in subvolcanic magma chambers. However, our data suggest that most VMS districts in this study, except Normétal and Val-d'Or, are dominated by quartz- and/or feldspar-phyric felsic lava flows or volcaniclastic rocks. The apparent inconsistency between phenocryst content, rhyolite type, and VMS favorability is difficult to explain with a model that involves a genetic link between deep petrogenetic processes for rhyolite generation and VMS formation. The most likely explanation is the presence of subvolcanic magma chambers above zones of magma generation, which would account for phenocryst formation. Such subvolcanic intrusions are well documented for most VMS districts in the Abitibi belt (Galley, 2003; Gaboury, 2006).

Fractionation pattern and style of volcanism

The FIII rhyolites are well known as volatile-poor rocks occurring in bimodal, basalt-rhyolite sequences (Lentz, 1998). These sequences, as exemplified by the Noranda and Matagami districts, are dominated by isolated to coalescent volcanic centers forming domes (e.g., cycle 3 of Noranda) and extensive flows (e.g., Watson Group of Matagami) with rare volcaniclastic horizons mainly of epiclastic origin (Table 1). Extensive cherty horizons or silicified tuffs indicating periods of volcanic quiescence are also typical of these sequences.

The FI rhyolites, which are at the other end of the fractionation spectrum, are poorly represented in the Abitibi belt. Volcanic rocks in the Bousquet district form a continuous compositional range from andesite to rhyodacite in volcaniclastic-dominated sequences (Table 1). Vesicularity is intense and quiescent periods (cherty horizons) have not yet been identified (Lafrance et al., 2003; Mercier-Langevin et al., 2007a). Other known FI rhyolites in the Superior province, such as at Obonga Lake (Tomlinson et al., 2002), in the Michipicoten belt (Sage et al., 1996), Meen-Dempster (Hollings et al., 2000), and in the North Caribou terrane (Hollings and Kerrich, 1999), are also dominantly tuffaceous but are not mineralized.

The FII rhyolites, characterized by a moderate fractionation pattern, are variably dominated by either volcaniclastic or coherent flow facies. The Val-d'Or and Selbaie districts are characterized by a continuous volcanic compositional range from andesite to rhyolite with large volumes of highly vesicular volcaniclastic rocks (Table 1). On the other hand, the Hunter district and the volcanic centers of the External North Volcanic zone are dominated by flow and lava domes of low vesicularity and bimodal composition (Table 1).

Fractionation pattern and style of mineralization

The VMS deposits associated with FIII rhyolites are typical "Noranda-type" deposits forming high-grade but relatively low-tonnage deposits (1–4 Mt), with the largest examples being Mattagami Lake (25.6 Mt) and Quémont (13.8 Mt). A major exception to this trend is the giant 240-Mt Kidd Creek VMS deposit in Ontario, which is also genetically related to FIIIb rhyolites (Lesher et al., 1986).

The gold-rich Horne deposit, the largest VMS in the Noranda district, features replacement-style mineralization in strongly sericitized felsic volcaniclastic rocks (Table 2). Some of the host rhyolites are FII type with calc-alkaline affinity, as previously documented by MacLean and Hoy (1991). The presence of more than one rhyolite type may be explained by the fact that the Horne mine is part of a different block than the felsic rocks of the central Noranda district (Kerr and Gibson, 1993). The Horne block is interpreted as a parallel rift environment to the central cauldron (Kerr and Gibson, 1993) or the top of the proposed New Senator caldera (Pearson and Daigneault, 2009).

Deposits associated with FI rhyolites are commonly atypical Cu-Au–rich deposits, ranging in style from sulfide-rich quartz veins to disseminations to sulfide replacements of permeable rocks (Table 2). Striking examples are the VMS deposits in the Bousquet area. Mineralization occurs mainly as massive sulfide replacements within highly permeable and highly vesicular volcaniclastic rocks. Well-defined Cu-rich stringer zones in the chlorite-altered feeder pipes of stratiform lenses are absent in many cases (Table 2). Aluminous alteration in the Cu-Au deposits at Dumagami, Bousquet 1 and 2, and Laronde (zone 20) has been compared to high-sulfidation alteration in epithermal Cu-Au deposits (Sillitoe et al., 1996; Hannington et al., 1999b; Dubé et al., 2007).

Mineralization associated with FII rhyolites is quite variable (Table 2). In the Selbaie area, mineralization occurs as copper-rich stringers and zinc-rich disseminations with poorly developed stratiform mineralization (Table 2). In the Val-d'Or

district, VMS deposits form large accumulations of disseminated sulfides with low Cu and Zn grades replacing permeable volcaniclastic horizons (except for the Louvicourt deposit) and lack well-defined underlying chloritic and Cu-rich zones (Table 2). In the Hunter district, mineralization hosted by FII rhyolite is more similar to that associated with FIII rhyolite, in that small massive sulfide lenses of exhalative origin accumulated at the top of the volcanic sequence along with banded iron formations during the waning stage of submarine volcanic activity (Table 2). Well-developed discordant sulfide stringers and chlorite alteration zones are also associated with these deposits (Table 2).

Summary and Conclusions

Rhyolites cover a complete spectrum of geochemical fractionation patterns that can be conveniently subdivided into informal FI-FII-FIII types. Furthermore, there is a complete spectrum of VMS deposits in terms of volcanic facies associations, base metal and gold contents, and alteration characteristics (Table 3). It emerges that there are no objectively barren rhyolite types, and that beyond any petrogenetic considerations involving the depth of felsic magma generation, other factors must be taken into account to explain the full spectrum of variations between geochemical signatures and volcanogenic hydrothermal activity.

Possible factors are temperature, viscosity, and volatile content, all of which have a profound influence on the volcanic products and consequently on the volcanic architecture (Touret, 1999). Submarine volcanic architecture in turn reflects the growth history, topography, effusive rate, bathymetry, and possible eruptive interference from other proximal volcanic centers (Cas, 1992; Gibson et al., 1999).

TABLE 3. Style of Volcanism and Mineralization Associated with Different Rhyolite Types

Group	Volcanism style	Mineralization style
FIII	Bimodal Low volatile content Domes and flows Low vesicularity index Few volcaniclastic rocks Exhalite-chert: common	Exhalative stratiform lenses High grade, low tonnage Cu-Zn ± Ag ± Au Discrete alteration pipe and Cu-rich stringer zone Examples: Quémont Mattagami Lake Ansil
FII	Similar to FIII-type	Similar to "FIII-type" Examples: Lyndhurst Hunter mine Gemini
	Similar to FI-type	Similar to "FI-type" Examples: Selbaie Manitou-Barvue
FI	Continuum andesite to rhyolite Abundance of volcaniclastic rocks High vesicularity Exhalite-chert: absent	Atypical Cu-Au veins, disseminations and replacement of permeable volcaniclastic rocks Diffuse alteration Examples: Laronde Bousquet 1 and 2 Comtois

The favorability of FIII rhyolites is commonly explained by the rapid transfer of low-volatile magma to the surface, thus inducing high heat flow (cf. Lentz, 1998). The extensional setting, manifested by well-defined calderas, rifts, or grabens favors magma ascent and provides enhanced structural permeability for the convective hydrothermal system (e.g., Hart et al., 2004). The bimodal sequences, with multicycle volcanism and hiatuses in volcanic activity, provide enough time to accumulate significant quantities of sulfides on the sea floor, mainly by exhalative processes, with VMS deposits forming near-volcanic rhyolite lava flow centers and domes (Gibson et al., 1999).

The VMS deposits associated with FI rhyolites are commonly replacements of highly permeable volcaniclastic rocks. These rocks are the main products of explosive eruption of calc-alkaline magma with a high volatile content. In such cases of replacement-style mineralization, a hiatus in volcanic activity is not necessary to form a VMS deposit by sea-floor exhalation, and these sequences commonly lack evidence of long pauses in volcanic activity. In addition to forming abundant volcaniclastic rocks, the explosive volcanism may promote enhanced structural permeability and contribute to large variations in bathymetry and confining pressure. Deposits typically occur close to isolated volcanic vents, as exemplified by the Bousquet district (Lafrance et al, 2003) and the Géant Dormant gold deposit (Gaboury and Daigneault, 1999). The high gold content of many of these deposits has been interpreted as a consequence of a magmatic gold contribution (Hannington et al., 1999b, 2005; Gaboury et al., 2000; Mercier-Langevin et al., 2007b). It is well known that magmas similar in composition to FI-type rhyolites emplaced in a subaerial setting are favorable hosts for Cu-Au porphyry deposits (Reich et al., 2003; Mungall, 2004).

It is noteworthy that FII sequences represent about 70 percent of rhyolites by surface area in the Abitibi (Pearson, 2005). For these moderately fractionated rhyolites, the trace element approach has some limitations when assessing relative prospectivity. Mineralized FII rhyolites, such as those of Val-d'Or, Selbaie, and Bousquet, have volcanic facies and mineralizing characteristics that are more similar to FI sequences, whereas those of the Hunter, Gemini-Turgeon, and External North Volcanic zone districts share characteristics with the FIIIa sequences, such as those of Noranda (Tables 3, 4). The FII sequences appear to be the most favorable hosts for VMS deposits when the volcanic style is dominated by highly vesicular volcaniclastic rocks derived by continuous fractionation from andesite to rhyolite. Conversely, those sharing characteristics of the FIII rhyolites—such as low vesicularity and bimodal dome- and lava flow-dominated sequences in the Hunter, External North Volcanic zone and Gemini-Turgeon districts—host "Noranda-type" deposits but appear less prospective.

The FI rhyolites appear highly favorable for VMS deposits but host styles of mineralization that differ from the classic strata-bound VMS lenses, including gold-bearing, sulfide-rich quartz veins, disseminations, and replacement-type sulfide lenses. A similar conclusion was reached by Mercier-Langevin et al. (2007b) based on their study of felsic rocks at the Laronde mine. Some FII rhyolites have a high potential to host VMS, such as Val-d'Or and Selbaie, whereas others,

such as in the Hunter, External North Volcanic zone, and Gemini-Turgeon districts, appear only weakly mineralized. The FII sequences host either Noranda-type VMS associated with flow-dome complexes or disseminated sulfide replacements and veins in dominantly volcaniclastic rocks. Volcaniclastic rocks appear to be the most favorable host for large-tonnage deposits and provide an important guide for exploration. The dominance of highly prospective FIII rhyolites in very large felsic centers, such as Noranda and Matagami, is a less useful exploration guide at the target scale. However, in small felsic centers that show an evolution from FIIIa to FII to FI, deposits are directly associated with FIIIa rhyolites, and their presence is thus a much more useful tool for targeting horizons with the greatest potential.

Acknowledgments

G. Bouchard of Xstrata Zinc (previously Noranda-Falconbridge) was instrumental to this study by suggesting it and providing technical support. P-L. Lajoie of the Université du Québec à Chicoutimi (UQAC) provided dedicated field assistance during the 2003 sampling program and sample preparations. J. Lavoie (UQAC) performed the petrographic study. This project benefited from numerous comments by representatives on the CONSOREM Research Committee. We also acknowledge CONSOREM for permission to publish this work. T. Gomwe of UQAC and V. Bodycomb of Vee Geoservices edited the English, and R. Daigneault of UQAC informally reviewed a preliminary version of the manuscript. The paper was substantially improved following reviews by T. Hart and P. Hollings. We are also grateful to M. Hannington for his constructive comments and efficient editorial work.

November 14, 2006; September 2, 2008

REFERENCES

Ayer, J., Amelin, Y., Corfu, F., Kamo, S., Ketchum, J., Kwok, K., and Trowell, N., 2002, Evolution of the southern Abitibi greenstone belt based on U-Pb geochronology; autochthonous volcanic construction followed by plutonism, regional deformation and sedimentation: Precambrian Research, v. 115, p. 63–95.

Ayer, J.A., Thurston, P.C., Bateman, R., Dubé, B., Gibson, H.L., Hamilton, M.A., Hathway, B., Hocker, S.M., Houlé, M.G., Hudak, G., Ispolatov, V.O., Lafrance, BLesher, C.M., MacDonald, P.J., Péloquin, A.S., Piercey, S.J., Reed, L.E., and Thompson, P.H., 2005, Overview of results from the Greenstone Architecture Project, Discover Abitibi Initiative: Geological Survey Open File Report 6154, 146 p.

Bandayera, D., Rhéaume, P., Doyon, J., and Sharma, K.N.M., 2004, Géologie de la région du lac Hébert (32G/03): Géologie Québec Report RG 2003-07, 58 p.

Barrett, T.J., and MacLean, W.H., 1994, Chemostratigraphy and hydrothermal alteration in exploration for VHMS deposits in greenstones and younger volcanic rocks: Geological Association of Canada, Mineral Deposits Division, Short Course Notes, v. 11, p. 433–467.

Barrie, C.T., and Davis, D.W., 1990, Timing of magmatism and deformation in the Kamiskotia-Kidd Creek area, western Abitibi subprovince, Canada: Precambrian Research, v. 46, p. 217–240.

Barrie, C.T., and Hannington.M.D., 1999, Classification of volcanic-associated massive sulfide deposits based on host-rock composition: Economic Geology Monograph 10, p. 1–11.

Barrie, C.T., and Krogh, T.E., 1996, U-Pb zircon geochronology of the Selbaie Cu-Zn-Ag-Au mine, Abitibi subprovince, Canada: Economic Geology, v. 91, p. 563–575.

Barrie, C.T., Ludden, J.N., and Green, T.H., 1993, Geochemistry of volcanic rocks associated with Cu-Zn and Ni-Cu deposits in the Abitibi subprovince: Economic Geology, v. 88, p. 1341–1358.

Barrie, C.T., Cathles, L.M., and Erendi, A., 1999, Finite element heat and fluid-flow computer simulations of a deep ultramafic sill model for the giant Kidd Creek volcanic-associated massive sulfide deposit, Abitibi subprovince, Canada: Economic Geology Monograph 10, p. 529–540.

Beaudry, C., and Gaucher, E., 1986, Cartographie géologique dans la region de Matagami: Ministère de l'Energie et des Ressources Report MB 86-32.

Bleeker, W., Parris, R.R., and Sager-Kinsman, A., 1999, High-precision U-Pb geochronology of the Late Archean Kidd Creek deposit and Kidd volcanic complex: Economic Geology Monograph 10, p. 71–122.

Bonneau, R-M., 1992, Minéralisation cuprifère dans le groupe archéen de Hunter Mine; exemple de l'indice Richard et de la mine Lyndhurst, région de Rouyn-Noranda, Abitibi, Québec: Unpublished M.Sc. thesis, Ste-Foy, Quebec, Université Laval, 88 p.

Campbell, I.H., Coad, P., Franklin, J.M., Gorton, M.P., Scott, S.D., Sowa, J., and Thurston, P.C., 1982, Rare earth elements in volcanic rocks associated with Cu-Zn massive sulfide mineralization. A preliminary report: Canadian Journal of Earth Sciences, v. 19, p. 619–623.

Campbell, I.H., Lesher, C.M., Coad, P., Franklin, J.M., Gorton, J., and Thurston, P.C., 1984, Rare-earth element mobility in alteration pipes below massive sulfide deposits: Chemical Geology, v. 45, p. 181–202.

Card, K.D., 1990, A review of the Superior province of the Canadian Shield, a product of Archean accretion: Precambrian Research, v. 48, p. 99–156.

Cas, R.A.F., 1992, Submarine volcanism: Eruption styles, products, and relevance to understanding the host-rock succession to volcanic-hosted massive sulfide deposits: Economic Geology, v. 87, p. 511–541.

Chartrand, F., 1989, The Akasaba gold deposit: Geological Association of Canada-Mineralogical Association of Canada, Field Trip A7 Guidebook, p. 1–13.

Chartrand, F., and Cattalani, S., 1990, Massive sulfide deposits in Northwestern Quebec: Canadian Institute of Mines and Metallurgy Special Volume 43, p. 77–91.

Chown, E.H., Daigneault, R., Mueller, W., and Mortensen, J.K., 1992, Tectonic evolution of the North Volcanic zone, Abitibi belt, Quebec: Canadian Journal of Earth Sciences, v. 29, p. 2211–2225.

Daigneault, R., and Allard, G.O., 1990, Le Complexe du Lac Doré et son environnement géologique (Région de Chibougamau, sous-province de l'Abitibi): Ministère de l'énergie et des Ressources du Québec Report MM 89-03, 275 p.

Daigneault, R., Mueller, W.U., and Chown, E.H., 2004, Abitibi greenstone belt plate tectonics: the diachrononous history of arc development, accretion and collision, *in* Eriksson, P., Altermann, W., Nelson, D., Mueller, W., Catuneanu, O., and Strand, K., eds., Developments in Precambrian geology/Tempos of events in Precambrian time: Amsterdam, Elsevier, p. 88–103.

Davidson, C.J., Varnes, R., Brown, A.V., and Connell, R., 2004. Structural controls on sulfide deposition at the dyke-lave boundary, slow spreading ocean crust, Macquarie Island: Terre Nova, v. 16, p. 9–15.

Davis, D.W., David, J., Dion, C., Gouthier, J., Bandyayera, D., Rhéaume, P., and Roy, P., 2005, Datations U-Pb effectuées en support aux travaux de cartographie géologique et de compilation géoscientifique du SGNO (2003–2004): Géologie Québec Report RP 2005-02, 20 p.

Dimroth, E., Imreh, L., Rocheleau, M., and Goulet, N., 1982, Evolution of the south-central part of the Archean Abitibi belt, Quebec. Part I: Stratigraphy and paleogeographic model: Canadian Journal of Earth Sciences, v. 19, p. 1729–1758.

Dostal, J., and Mueller, W., 1996, An Archean oceanic felsic dyke swarm in a nascent arc: the Hunter mine group, Abitibi greenstone belt, Canada: Journal of Volcanology and Geothermal Research, v 72, p. 37–57.

Dubé, B., Mercier-Langevin, P., Hannington, M.D., Lafrance, B., Gosselin, P., and Gosselin, G., 2007, The LaRonde Penna world-class Au-rich volcanogenic massive sulfide deposit, Abitibi, Québec: Mineralogy and geochemistry of alteration and implications for genesis and exploration: Economic Geology, v. 102, p. 633–666.

Dupré, F., Jébrak, M., Faure, S., Rioppel, P., and Gaboury, D., 2002, The Comtois Cu-Au deposit, an unusual type of an Archean VMS [abs.]: Geological Association of Canada-Mineralogical Association of Canada Joint Annual Meeting, Saskatoon, May 28th, Abstracts, p. 31.

Franklin, J.M., Lydon J.W., and Sangster, D.F., 1981, Volcanic-associated massive sulfide deposits: Economic Geology 75th Anniversary Volume, p. 485–627.

Franklin, J.M., Gibson, H.L., Jonasson, I.R., and Galley, A.G., 2005, Volcanogenic massive sulfide deposits: Economic Geology 100th Anniversary Volume, p. 523–560.

Gaboury, D., 2006, Geochemical approaches in the discrimination of synvolcanic intrusions as a guide for volcanogenic base metal exploration: Example from the Abitibi belt, Canada: Applied Earth Science, v. 115, p. 71–79.

Gaboury, D., and Daigneault, R., 1999, Evolution from seafloor-related to sulfide-rich quartz vein-type gold mineralization during deep submarine volcanic construction: The Géant Dormant gold mine, Archean Abitibi belt, Canada: Economic Geology, v. 94, p. 3–21.

Gaboury, D., Daigneault, R., and Beaudoin, G., 2000, Volcanogenic-related origin of sulfide-rich quartz veins: Evidence from O and S isotopes at the Géant Dormant gold mine, Abitibi belt, Canada: Mineralium Deposita, v. 35, p. 21–36.

Galley, A.G., 2003, Composite synvolcanic intrusions associated with Precambrian VMS-related hydrothermal systems: Mineralium Deposita, v. 83, p. 443–473.

Gauthier, M., Baillargeon, F., and Legault, M., 2003, Etude des faciès sédimentaires et des faciès d'altération primaires du gisement d'or archéen d'Eagle-Telbel, canton de Joutel, Abitibi: Géologie Québec Report MB 2002-06, 33 p.

Gélinas, L., Trudel, P., and Hubert, C., 1984, Chemostratigraphic division of the Blake River Group, Rouyn-Noranda area, Abitibi, Quebec: Canadian Journal of Earth Sciences, v. 21, p. 220–231.

Gibson, H.L., 1990, The mine sequence of the central Noranda volcanic complex: Geology, alteration, massive sulphide deposits and volcanological reconstruction: Unpublished Ph.D. thesis, Ottawa, Ontario, Carleton University, 715 p.

Gibson, H.L., and Watkinson, D.H., 1990, Volcanogenic massive sulfide deposits of the Noranda cauldron and shield volcano, Quebec: Canadian Institute of Mines and Metallurgy Special Volume 43, p. 119–132.

Gibson, H.L., Morton, R.L., and Hudak, G.J., 1999, Submarine volcanic processes, deposits, and environments favorable for location of volcanic-associated massive sulfide deposits: Reviews in Economic Geology, v. 8, p. 13–51.

Gobeil, A., 1980, Etude lithogéochimique des roches volcaniques dans la région de la mine Lemoine, District de Chibougamau, Québec: Canadian Institute of Mining and Metallurgy Bulletin, v. 73, no. 817, p. 86–95.

——2006, Géologie et minéralisation du projet Gémini, secteur Casa Berardi [abs.]: Forum technologique du CONSOREM, August 31th, Rouyn-Noranda, Program and Abstracts, p. 21–22.

Goutier, J., and Melançon, M., 2007, Compilation géologique de la Sous-province de l'Abitibi (version préliminaire): Ministère des Ressources naturelles et de la Faune, Québec, scale 1/500,000.

Guha, J., Dubé, B., Pilote, P., Chown, E.H., Archambault, G., and Bouchard, G., 1988, Gold mineralization patterns in relation to the lithologic and tectonic evolution of the Chibougamau mining district, Quebec, Canada: Mineralium Deposita, v. 23, p. 293–298.

Hannington, M.D., Barrie C.T., and Bleeker, W., 1999a, The Giant Kidd Creek volcanogenic massive sulfide deposit, western Abitibi subprovince, Canada: Economic Geology Monograph 10, p. 1–30.

Hannington, M.D., Poulsen, K.H., Thompson, J.F.H., and Sillitoe, R.H., 1999b. Volcanogenic gold in massive sulfide environment: Reviews in Economic Geology, v. 8, p. 325–356.

Hannington, M.D., de Ronde, C.E.J., and Petersen, S., 2005, Sea-floor tectonics and submarine hydrothermal systems: Economic Geology 100th Anniversary Volume, p. 111–141.

Hart, T.R., Gibson, H.L., and Lesher, C.M., 2004, Trace element geochemistry and petrogenesis of felsic volcanic rocks associated with volcanogenic massive Cu-Zn-Pb sulfide deposits: Economic Geology, v. 99, p. 1003–1013.

Hollings, P., and Kerrich, R., 1999, Trace element systematics of ultramafic and mafic volcanic rocks from the 3 Ga North Caribou greenstone belt, Northwestern Superior province: Precambrian Research, v. 93, p. 257–279.

Hollings, P., Stott, G., and Wyman, D., 2000, Trace element geochemistry of the Meen-Dempster greenstone belt, Uchi subprovince, Superior province, Canada: Back-arc development on the margins of an Archean protocontinent: Canadian Journal of Earth Sciences, v. 37, p.1021–1038.

Jenkins, C.L., and Brown, A.C., 1999, Cadre métallogénique des gisements de sulfures massifs volcanogènes et filoniens aurifères des cantons Bourlamaque et Louvicourt, partie sud de la Sous-province de l'Abitibi: Géologie Québec Report MB 99-12, 42 p.

Kerr, D.J., and Gibson, H.L., 1993, A comparison of the Horne volcanogenic massive sulfide deposit and intracauldron deposits of the Mine Sequence, Noranda, Quebec: Economic Geology, v. 88, p. 1419–1442.

Kerrich, R., and Wyman, D.A., 1997, Review of development in trace-element fingerprinting of geodynamic settings and their implications for mineral exploration: Australian Journal of Earth Sciences, v. 44, p. 465–487.

Labbé, J.-Y., 1999, Evolution stratigraphique et structurale dans la région d'Amos-Barraute: Géologie Québec Report ET-98-04, p. 5–18.

Labbé, J.-Y., and Couture, F., 1999, Contexte géologique des minéralisations métalliques, région d'Amos-Barraute: Géologie Québec Report ET-98-04, p. 19–36.

Lacroix, J., Daigneault, R., Chartrand, F., and Guha, J., 1993, Structural evolution of the grevet Zn-Cu massive sulfide deposit, Lebel-sur-Quévillon area, Abitibi subprovince, Quebec: Economic Geology, v. 88, p. 1559–1577.

Lacroix, S., 1998, Compilation et répartition des gisements polymétalliques à tonnage évalué dans la Sous-province de l'Abitibi: Ministère des Ressources naturelles du Québec Report MB 98-06, p. 29.

Lafrance, B., 2003, Reconstruction d'un environnement de sulfures massifs volcanogènes déformé: Exemple archéen de Normétal, Abitibi: Unpublished Ph.D. thesis, Chicoutimi, Québec, Université du Québec à Chicoutimi, 362 p.

Lafrance, B., Mueller W.U., Daigneault, R., and Dupras, N., 2000, Evolution of a submerged composite arc volcano: Volcanology and geochemistry of the Normétal volcanic complex, Abitibi greenstone belt, Québec, Canada: Precambrian Research, v. 101, p. 277–311.

Lafrance, B., Moorhead, J., and Davis, D.W., 2003, Cadre géologique du camp minier de Doyon-Bousquet-LaRonde: Géologie Québec Report ET 2002-07, 43 p.

Larsen, J.E., and Hutchinson, R.W., 1993, The Selbaie Zn-Cu-Ag deposits, Quebec, Canada: An example of evolution from subaqueous to subaerial volcanism and mineralization in an Archean caldera environment: Economic Geology, v. 88, p. 1460–1482.

Lavallière, G., 1995, Processus de formation et implications pour l'exploration des cheminées atypiques des gisements volcanogènes de Matagami: Unpublished Ph.D. thesis, Chicoutimi, Québec, Université du Québec à Chicoutimi, 451 p.

Legault, M., Gauthier, M., Jébrak, M., Davis D.W., and Baillargeon, F., 2002, Evolution of the subaqueous to near-emergent Joutel volcanic complex, North Volcanic zone, Abitibi subprovince, Quebec, Canada: Precambrian Research, v. 115, p. 187–221.

Lentz, D.R., 1998, Petrogenetic evolution of felsic volcanic sequences associated with Phanerozoic volcanic-hosted massive sulphide systems: the role of extensional geodynamics: Ore Geology Reviews, v. 12, p. 289–327.

Lesher, C.M., Goodwin, A.M., Campbell, I.H., and Gorton, M.P., 1986, Trace-element geochemistry of ore-associated and barren, felsic metavolcanic rocks in the Superior province, Canada: Canadian Journal of Earth Sciences, v. 23, p. 222–237.

Lydon, J.W., 1984, Ore deposit models: Volcanogenic massive sulfide deposits. Part 1: A descriptive model: Geoscience Canada, v. 11, p. 195–202.

MacLean, W.H., 1988, Rare earth elements mobility at constant inter-REE ratios in the alteration zone at the Phelps Dodge massive sulfide deposit, Matagami, Quebec: Mineralium Deposita, v. 23, p. 231–238.

MacLean, W.H., and Hoy, L.D., 1991, Geochemistry of hydrothermally altered rocks at the Horne mine, Noranda, Quebec: Economic Geology, v. 86, p. 506–528.

Mercier-Langevin, P., 2005, Géologie du gisement de sulfures massifs volcanogènes aurifères de LaRonde, Abitibi, Québec: Unpublished Ph.D. thesis, Laval-INRS Universities, 694 p.

Mercier-Langevin, P., Dubé, B., Hannington, M.D., Davis, D.W., Lafrance, B., and Gosselin, G., 2007a, The LaRonde Penna Au-rich volcanogenic massive sulfide deposit, Abitibi greenstone belt, Quebec: Part I. Geology and geochronology: Economic Geology, v. 102, p. 585–609.

Mercier-Langevin, P., Dubé, B., Hannington, Richer-Laflèche, M., and Gosselin, G., 2007b, The LaRonde Penna Au-rich volcanogenic massive sulfide deposit, Abitibi greenstone belt, Quebec: Part II. Lithogeochemistry and paleotectonic setting: Economic Geology, v. 102, p. 611–631.

Mortensen, J.K., 1993, U-Pb geochronology of the eastern Abitibi subprovince: Part 1: Chibougamau-Matagami-Joutel: Canadian Journal of Earth Sciences, v. 30, p. 11–28.

Morton, R.L., and Franklin, J.M., 1987, Two-fold classification of Archean volcanic-associated massive sulfide deposits: Economic Geology, v. 82, p. 1057–1063.

Mueller, W., and Donaldson, J.A., 1992, A felsic feeder dyke swarm formed under the sea: the Archean Hunter mine group, south-central Abitibi belt, Quebec, Canada: Bulletin of Volcanology, v. 54, p. 602–610.

Mueller, W.U., and Mortensen, J.K., 2002. Age constraints and characteristics of subaqueous volcanic construction, the Archean Hunter mine group, Abitibi greenstone belt: Precambrian Research, v. 115, p. 119–152.

Mueller, W., Daigneault, R., Mortensen, J., and Chown, E.H., 1996, Archean terrane docking: Upper crust collision tectonics, Abitibi greenstone belt, Quebec, Canada: Tectonophysics, v. 265, p. 127–150.

Mueller, W.U., Stix, J.B., White, J.D.L., Corcoran, P.L., Lafrance, B., and Daigneault, R., 2008, Characterisation of Archean subaqueous calderas in Canada: Physical volcanology, carbonate-rich hydrothermal alteration and new exploration model: Developments in Volcanology, v. 10, p. 181–232.

Mungall, J.E., 2004. Roasting the mantle: Slab melting and the genesis of major Au and Au-rich Cu deposits: Geology v. 32, p. 915–918.

Nakamura, N., 1974, Determination of REE, Ba, Fe, Mg, Na, K in carbonaceous and ordinary chondrites: Geochimica et Cosmochimica Acta, v. 38, p. 757–775.

Pearson, V., 2005, Classification géochimique des environnements volcaniques felsiques favorables–Phase II. Projet 2004-2: Rapport CONSOREM, 27 p.

Pearson, V., and Daigneault, R., 2009, Evolution of an Archean megacaldera cluster: the Blake River Group, Abitibi subprovince: Precambrian Research, v. 168, p. 66–82.

Peloquin, A.S., Verpaelst, P., and Ludden, J.N., 1996, Spherulitic rhyolites of the Archean Blake River Group, Canada: Implications for stratigraphic correlation and volcanogenic massive sulfide exploration: Economic Geology, v. 91, p. 343–354.

Piché, M., Guha, J., and Daigneault, R., 1993, Stratigraphic and structural aspects of the volcanic rocks of the Matagami mining camp, Quebec: Implications for the Norita ore deposit: Economic Geology, v. 88, p. 1542–1558.

Pilote, P., Robert, F., Kirkham, R.V., Daigneault, R., and Sinclair, W.D., 1998, Minéralisations de type porphyrique et filoniennes dans le Complexe du lac Doré - les secteurs de lac Clark et de l'Ile Merrill: Ministère Ressources naturelles Québec, Report DV 98-03, p. 71–90.

Pilote, P., Scott, C., Mueller, W.U., Lavoie, S., and Riopel, P., 1999, Géologie des formations Val-d'Or, Héva et Jacola: Nouvelle interprétation du Groupe de Malartic: Ministère de l'Énergie et des Ressources du Québec Report DV 99-03, 52 p.

Prior, G.J., Gibson, H.L., Watkinson, D.H., Cook, R.E., and Hannington, M.D., 1999, Rare earth and high field strength element geochemistry of the Kidd Creek rhyolites, Abitibi greenstone belt, Canada: Evidences for Archean felsic volcanism and massive sulfide ore formation in an Icelandic-style environment: Economic Geology Monograph 10, p. 457–484.

Reich, M., Parada, M.A., Palacious, C., Dietrich, A., Schultz, F., and Lehmann, B., 2003, Adakite-type signature of late Miocene intrusions at the Los Pelambres giant porphyry copper deposit in the Andes of central Chile: Metallogenic implications: Mineralium Deposita, v. 38, p. 876–885.

Rodney, A.L., PAR Weihed, and The Global VMS Research Project Team, 2002, Global comparaisons of volcanic-associated massive sulphide districts: Geological Society of London Special Publication 204, p. 13–37.

Sage, R.P., Lightfoot, P.C., and Doherty, W., 1996, Bimodal cyclical Archean basalts and rhyolites from the Michipicoten (Wawa) greenstone belt, Ontario: Geochemical evidence for magma contributions from the asthenospheric mantle and ancient continental lithosphere near the southern margin of the Superior province: Precambrian Research, v. 76, p. 119–153.

Scott, C.R., Mueller, W.U., and Pilote, P., 2002, Physical volcanology, stratigraphy, and lithogeochemistry of an Archean volcanic arc: Evolution from plume-related volcanism to arc rifting of SE Abitibi greenstone belt, Val-d'Or, Canada: Precambrian Research, v. 115, p. 223–260.

Sharpe, J.L., 1968, Géologie et gisements de sulfures de la région de Matagami, Comté d'Abitibi-Est: Ministère des Ressources naturelles Report 137.

Sillitoe, R.H., Hannington, M.D., and Thompson, J.F.H., 1996, High-sulfidation deposits in the volcanogenic massive sulfide environment: Economic Geology, v. 91, p. 204–212.

Sun, S.-S., and McDonough, W.F., 1989, Chemical and isotopic systematics of oceanic basalts: Implications for mantle composition and processus: Geological Society of America Special Publication 42, p. 399–444.

Taner, M.F., 2000, The geology of the volcanic-associated polymetallic (Zn, Cu, Ag and Au) Selbaie deposits, Abitibi, Quebec, Canada: Exploration and Mining Geology, v. 9, p. 189–214.

Thurston, P.C., 1981, Economic evaluation of Archean felsic volcanic rocks using REE geochemistry: Geological Society of Australia Special Publication 7, p. 439–450.

Tomlinson, K.Y., Davis, D.W., Percival, J.A., Hughes, D.J., and Thurston, P.C., 2002, Mafic to felsic magmatism and crustal recycling in the Obonga Lake greenstone belt, Western Superior province: Evidence from geochemistry, Nd isotopes and U-Pb geochronology: Precambrian Research, v. 114, pp. 295–325.

Touret, J.-C., 1999, Volcanic geomorphology—an overview: Earth-Sciences Review, v. 47, p. 95–131.

Tremblay, A., Maisonneuve, S., and Lacroix, S., 1996, Contexte lithologique et structural des gîtes de Duvan et de DuReine, région de La Sarre, Abitibi, Québec: Géologie Québec Report MB 96-36, 66 p.

Vorobiev, L., 2000, Minéralisation aurifère de type skarn dans le secteur d'Akasaba, formation de Héva: Géologie Québec Report MB 2000-9, p. 87–95.

Wyman, D.A., Kerrich, R., and Polat, A., 2002 Assembly of Archean cratonic mantle lithosphere and crust: Plume-arc interaction in the Abitibi-Wawa subduction-accretion complex: Precambrian Research, v. 115, p. 37–62.

Zhang, P.L., Machado, N., Ludden, J., and Moore, D., 1993, Geotectonics constraints from U-Pb ages for the Blake River Group, the Kinojévis Group and the Normétal mine area, Abitibi, Québec [abs.]: Geological Association of Canada-Mineralogical Association of Canada Joint Annual Meeting, Edmonton, Program and Abstracts, v. 18, p. A114.

APPENDIX 1

Analytical Results for Felsic Volcanic Rocks of the Abitibi Belt

Number	R-1	R-2	R-3	R-4	R-5	R-6	R-8	R-9	R-10	R-11	R-12	R-13	R-14	R-15	R-16	R-17	R-18
Zone	18	18	18	18	18	18	18	18	18	18	18	18	18	18	18	18	18
UTME	340297	340432	358939	379501	377993	377836	362103	360550	305875	297896	308145	309450	309026	308708	310044	310158	312853
UTMN	5444424	5444249	5432783	5455516	5456121	5456351	5454944	5446415	5329342	5327748	5328321	5326227	5324932	5327946	5330413	5330994	5328363
SiO_2 (wt %)	69.39	72.47	67.43	83.37	85.95	71.21	69.12	78.17	85.17	67.69	67.78	59.03	79.57	65.25	68.14	70.86	75.8
Al_2O_3	15.58	14.67	15.81	8.44	6.45	15.14	12.03	11.98	6.56	15.41	14.54	12.61	8.9	14.41	11.23	13.98	14.38
TiO_2	0.23	0.15	0.28	0.19	0.16	0.22	0.52	0.23	0.09	0.4	1.1	0.91	0.57	0.76	0.47	0.45	1.07
Fe_2O_3	2.37	1.04	3.4	2.07	3.65	1.66	6.02	0.7	3.08	2.63	1.86	9.8	2.85	6.2	4.42	2.45	1.78
MgO	0.52	0.4	0.24	0.12	0.44	0.34	0.72		0.78		0.21	2.12	1.18	6.3	2.77	1.25	0.19
MnO	0.07	0.01	0.08	0.05	0.02	0.03	0.1	0.02		0.05	0.05	0.12	0.05	0.1	0.15	0.03	0.02
K_2O	1.52	1.81	1.42	0.66	1.24	2.02	1.47	1.42	1.5	0.57	1.37	0.11	0.02	2.32	0.88	0.41	4.35
CaO	1.39	3.29	3.43	0.5	0.03	1.85	2.48	0.51		9.08	3.95	6.57	2.35	0.52	4.26	2.85	0.33
Na_2O	6.29	4.11	4.08	3.55	0.28	4.96	4.25	5.38	0.15	2.33	5.02	4.64	3.49	0.31	2.95	5.82	0.27
P_2O_5	0.11	0.07	0.07	0.03	0.02	0.05	0.07	0.04	0.02	0.2	0.23	0.2	0.13	0.34	0.1	0.27	0.25
LOI	1.63	1.8	4.25	0.82	1.43	2.39	2.95	0.91	2.18	0.93	3.51	5.03	0.96	4.21	5.1	1.39	1.96
Total	99.08	99.83	100.49	99.79	99.66	99.86	99.74	99.32	99.53	99.28	99.63	101.14	100.05	100.71	100.47	99.77	100.39
Ce (ppm)	32.4	48.06	11.03	48.65	37.13	12.51	99.57	98.33	43.57	49.41	51.72	45.84	23.7	54.98	27.48	60.98	40.16
Cs	0.987	1.348	1.582	0.188	0.458	0.988	1.128	0.555	0.656	0.197	1.651	0.21	0.029	1.371	0.405	0.176	4.185
Dy	1.347	1.439	0.922	9.46	8.704	0.932	18.188	12.118	3.669	4.425	6.256	17.446	3.039	3.86	4.434	5.531	5.851
Er	0.863	0.847	0.526	6.146	6.212	0.544	12.28	6.619	2.425	2.748	3.888	11.603	1.877	2.047	2.94	3.37	3.517
Eu	0.609	0.821	0.415	2.417	0.999	0.375	2.825	2.139	1.129	1.198	1.521	2.813	0.543	1.092	0.897	1.283	1.451
Gd	1.669	1.983	1.148	9.629	5.921	1.141	15.849	12.52	4.548	5.709	6.877	15.044	3.303	5.523	4.294	6.954	7.018
Hf	3.8	3.7	2.2	7.8	8.4	2.9	13	10.7	4.1	6.8	8.1	9.1	3.5	6.1	5.1	7.7	6.3
Ho	0.281	0.282	0.181	2.012	1.975	0.181	3.983	2.384	0.778	0.89	1.278	3.83	0.626	0.719	0.957	1.111	1.177
La	15.86	23.54	5.42	20.09	9.26	6.23	43.01	41.37	17.84	19.26	20.76	16.56	9.44	21.97	10.98	24.08	15.08
Lu	0.153	0.149	0.073	0.928	0.918	0.081	1.814	0.872	0.397	0.474	0.556	1.783	0.287	0.307	0.467	0.587	0.556
Nb	3.4	3.6	1.7	18.2	17.2	2.1	35.2	22.2	4.7	8.5	10.1	12.8	4.4	8.3	6.4	10.2	8
Nd	14.99	21.69	5.56	31.54	15.47	6.02	56.66	54.48	25.29	30.4	31.84	37.21	14.18	33.44	16.96	37.88	28.21
Pr	4.062	5.986	1.35	6.915	3.466	1.499	13.188	12.932	5.856	6.993	7.151	7.262	3.263	7.637	3.871	8.654	5.947
Rb	34.1	35.47	45.29	18.67	35.79	50.82	37.4	25.46	21.67	12.4	39	2.07	0.32	42.39	17.81	11.48	96.01
Sm	2.35	3.14	1.22	8.26	4.31	1.23	13.96	12.22	5.76	6.9	7.3	11.56	3.37	7.15	4.04	8.34	7.1
Sr	431.7	327.8	338.6	43.5	62	207.6	93.5	64.4	13.4	163.7	98.5	179.4	46.4	27.3	72.6	174.9	60
Ta	0.29	0.3	0.2	1.12	1.11	0.24	2.08	1.42	0.44	0.6	0.66	0.84	0.35	0.54	0.44	0.67	0.58
Tb	0.232	0.263	0.166	1.539	1.212	0.164	2.801	2.015	0.62	0.8	1.048	2.645	0.503	0.72	0.708	0.965	1.015
Th	2.15	2.67	0.8	2.07	2.67	1.07	4.84	4.28	2.4	4.04	3.53	1.54	1.54	3.2	1.9	4.48	3.39
Tm	0.134	0.13	0.074	0.923	0.945	0.079	1.836	0.959	0.382	0.434	0.571	1.746	0.276	0.303	0.446	0.525	0.518
U	0.475	0.572	0.34	0.499	0.693	0.357	1.244	0.808	0.513	0.901	0.87	0.416	0.416	0.707	0.507	0.95	1.323
Y	7.89	8.26	5.01	59.18	51.94	5.24	109.31	54.74	19.87	25.55	35.6	101.48	17.49	19.89	26.11	31.31	33.14
Yb	0.93	0.92	0.49	6.11	6.18	0.53	12.06	6.15	2.56	3.04	3.77	11.6	1.83	2.04	3.01	3.63	3.49
Zr	154.3	143	77.1	301.3	308.5	98.1	475.1	402.1	126.5	262.2	302.4	318	130.7	232.2	188	290.5	230.2
Be	0.7	0.56	0.6	0.74	1.29	0.92	1.82	0.88	0.33	0.92	0.83	0.55	0.25	1.13	0.39	0.92	1.2
Co	2.07	2.63	5.94	0.43	1.61	2.26	5.31	0.16	4.58	1.2	5.15	10.34	9.06	14.91	8.34	5.42	2.13
Cu	47.32	6.96	23.56	6.64	27.82	3	9.11	23.07	68.87	6.1	103.5	19.52	13.66	3.42	73.02	3.59	23.93
Li	53	26	14	1	3	2	13	4	4	3	7	25	2	43	18	8	8
Ni	10.37	4.76	15.58	6.02	7.6	9.17	5.34	2.9	4.19	4.71	7.46	13.45	45.59	41.33	8.39	8.87	2.41
Sc	2.8	1.9	5.4	2.1	1.1	2.7	6.7	2.9	7.1	8.5	12.1	18.2	14.5	9.6	12.5	13.2	22.2
V	9.06	5.24	58.94	1.95	2.14	25.94	20.9	2.05	1.4	35.44	133.7	61.08	118.93	88.77	56.68	49.44	113.41
Zn	43.77	10.05	51.12	83.77	136	10.34	72.54	39.11	62.76	8.54	41.36	58.48	46.45	192	69.8	11.99	16.91
Ba	368.24	698.23	297.04	115.16	402.28	425.84	309.43	312.31	346.45	227.2	318.3	145.9	3.68	328	136.1	145.48	373.75
Cd	0.054	0.052	0.035	0.108	0.113	0.031	0.122	0.099	0.046	0.124	0.072	0.095	0.046	0.08	0.058	0.054	0.053
Cr	46	37.41	62.47	34.97	30.46	27.22	13.72	11.94	12.64	11.92	24.36	60.2	48.28	86.95	22.51	22.05	9.78
Ga	18.64	16.39	17.7	9.85	15.82	19.49	27.03	19.47	10.91	24.1	17.04	20.61	10.26	17.78	14.01	14.58	15.18
Mo	5	5	3.14	3.17	3.16	1.79	1.39	0.85	3.08	0.74	1.06	0.5	1.95	0.22	0.35	0.88	1.09
Pb	3.8	2.5	3.8	6.1	11.7	2.6	2.3	2.4	22.5	27.9	3.6	1.8	1.4	6.5	1.8	1.4	5.8
Sn	0.9	1	1.12	2.51	4.06	1.06	5.44	5.34	3.31	2.54	2.4	2.16	0.87	1.98	1.81	1.69	2.02
Tl	0.21	0.22	0.17	0.08	1.92	0.28	0.09	0.07	0.63	0.03	0.15	0.01		0.1	0.05	0.03	0.27
W	0.73	0.48	0.18	0.21	0.42	1.8	0.8	0.86	0.54	0.5	0.79	0.48	0.72	0.69	0.56	0.18	1.07

APPENDIX 1 *(Cont.)*

Number	R-19	R-20	R-21	R-22	R-23	R-25	R-26	R-27	R-28	R-29	R-30	R-31	R-32	R-34	R-35	R-36	R-37
Zone	18	18	18	18	17	17	17	18	17	17	17	17	17	17	17	17	17
UTME	323164	311601	303148	302480	718033	716415	716415	296027	711276	701359	700608	684422	681858	619401	618604	617237	615340
UTMN	5326912	5330063	5367105	5377870	5381228	5387455	5387447	5399513	5388917	5393938	5388487	5389578	5394610	5429078	5429499	5430259	5416389
SiO_2 (wt %)	75.41	69.33	81.76	69.52	55.13	77.61	70.65	74.72	54.59	65.8	60.24	62.11	62.88	83.64	88.82	75.39	64.65
Al_2O_3	12.21	14.24	6.87	12.33	16.36	12.44	13.55	12.56	16.19	15.57	15.64	13.98	17.16	10.99	9.74	13.56	17.5
TiO_2	0.66	0.6	0.11	0.37	0.7	0.2	0.32	0.17	0.86	0.79	0.54	0.76	0.25	0.16	0.05	0.56	0.35
Fe_2O_3	5.96	4.56	5.56	3.49	8.31	0.23	4.38	2.8	9.15	2.84	7.14	5.59	1.85	0.97	0.02	2.96	3.96
MgO	1.87	4.15	0.22	0.89	5.62		0.68	0.71	4.93	0.95	3.94	3.1	0.98	0.54		1.32	2.24
MnO	0.12	0.03		0.11	0.13		0.03	0.05	0.15	0.08	0.11	0.07	0.02	0.01		0.06	0.09
K_2O	1.39	2.94	2.2	2.17	1.61	1.95	2.36	1.22	0.72	2.65	1.32	1.75	4.14	2.18	0.53	3.01	1.82
CaO	0.15	0.44	0.02	3.62	5.79	1.23	2.41	0.7	8.71	5.6	7.56	4.54	3.77	0.03	0.03	0.18	2.68
Na_2O		0.43	0.1	1.14	2.72	4.05	2.05	5.41	1.86	4.58	2.27	2.43	4.25	0.77	0.05	0.24	4.87
P_2O_5	0.12	0.3	0.01	0.12	0.14	0.03	0.07	0.03	0.14	0.18	0.11	0.14	0.08	0.02	0.02	0.11	0.12
LOI	2.39	3.38	3.72	6.14	2.9	1.72	3.54	1.08	3.39	0.63	2.09	5.98	4.48	1.66	0.42	2.22	1.98
Total	100.19	100.4	100.58	99.91	99.4	99.45	100.04	99.45	100.7	99.65	100.96	100.45	99.86	100.98	99.65	99.62	100.26
Ce (ppm)	7.23	29.74	22.36	54.42	33.9	59.44	73.91	116.95	27.28	53.2	28.61	34.5	17.94	19.88	18.19	32.51	35.98
Cs	0.921	0.918	0.513	1.533	1.645	0.952	2.53	0.936	0.905	0.134	0.645	1.292	2.364	1.71	0.086	1.036	3.115
Dy	1.08	2.502	4.629	6.048	3.773	6.349	7.867	13.788	3.62	5.977	2.994	3.584	0.737	4.66	8.796	6.93	0.921
Er	0.831	1.671	3.915	3.963	2.243	3.436	4.932	8.121	2.228	3.642	1.8	2.196	0.334	3.037	6.193	4.302	0.408
Eu	0.228	0.807	0.666	1.757	1.07	1.073	1.377	1.428	1.126	1.527	0.761	0.975	0.496	0.452	0.273	0.481	0.737
Gd	1.226	3.668	3.759	6.535	3.933	6.867	7.796	14.022	3.725	5.863	3.063	3.798	1.239	3.583	6.341	5.589	1.702
Hf	3.3	5.4	6.6	6.6	4.1	6.1	7.1	8.3	3.3	6.6	3.4	4.9	2.3	4.8	4	7.3	2.7
Ho	0.249	0.512	1.123	1.284	0.772	1.222	1.633	2.765	0.756	1.241	0.609	0.748	0.127	0.999	1.979	1.447	0.156
La	2.66	10.76	9.63	22.82	14.64	27.85	34.05	53.09	11.95	24.92	12.97	15.45	8.44	7.31	6.78	13.13	16.74
Lu	0.174	0.352	0.787	0.65	0.335	0.495	0.766	1.25	0.324	0.543	0.266	0.316	0.042	0.487	0.966	0.618	0.052
Nb	4	8.3	12.9	11.2	7.2	10.9	13.6	23.9	6	10.7	5.9	8.1	2.2	10	15.3	12.1	2.6
Nd	5.63	17.7	12.96	31.42	17.32	28.8	34.35	58.71	14.72	25.46	13.83	17	8.78	8.4	12.37	15.97	16.92
Pr	1.127	3.881	2.961	7.289	4.296	7.175	8.759	14.652	3.513	6.369	3.439	4.195	2.215	2.117	2.648	4.11	4.467
Rb	23.16	58.06	39.02	48.21	58.76	41.33	45.86	41.41	19.15	48.5	39.28	48.34	75.57	68.94	6.97	41.84	47.88
Sm	1.41	4.22	3.23	7.25	3.82	6.7	7.68	13.47	3.35	5.58	2.98	3.71	1.7	2.34	4.46	4.46	2.71
Sr	242.2	49.8	15.1	226	255.6	70.6	78.9	54	208.1	133.1	159.5	115.3	213.5	42.9	1	37.1	417.4
Ta	0.33	0.55	0.96	0.81	0.6	1.14	1.33	1.99	0.48	0.91	0.53	0.66	0.22	0.86	1.43	0.9	0.22
Tb	0.177	0.47	0.661	0.974	0.623	1.087	1.277	2.279	0.602	0.974	0.503	0.603	0.155	0.709	1.283	1.091	0.199
Th	1.03	1.52	1.35	3.2	1.48	5.99	7.82	8.67	1.31	3.83	1.81	2.37	1.39	2.91	5.63	2.86	2.7
Tm	0.138	0.27	0.664	0.613	0.336	0.502	0.749	1.223	0.321	0.54	0.262	0.319	0.046	0.465	0.963	0.631	0.055
U	0.38	0.666	0.654	0.932	0.508	1.17	0.739	2.136	0.34	1.046	0.476	0.75	0.491	0.982	0.504	0.892	0.898
Y	6.69	13.73	31.77	35.06	21.38	29.61	45.83	72.29	20.62	34.39	17.04	20.46	3.47	28.5	56.4	38.92	4.24
Yb	1.02	2.03	4.84	4.23	2.22	3.31	5.01	8.34	2.11	3.54	1.73	2.06	0.3	3.13	6.37	4.1	0.36
Zr	121.5	204.7	215.4	251.9	164.5	205.7	240.6	247.3	132.5	257.5	138.6	199	87.9	159	79.4	294.3	103.8
Be	0.47	1.3	0.2	0.81	0.63	0.94	0.79	1.14	0.49	0.61	0.54	0.71	1.05	0.96	0.1	1	0.94
Co	9.46	4.6	5.13	2.75	35.94	1.1	2.82	1.73	31.06	6.81	29.51	20.88	5.86	0.9	2	1.16	10.41
Cu	2604	8.24	9.41	14.87	51.43	2.27	12.48	20.46	41.56	40.73	58.69	41.48	3.84	5.07	1.18	2.7	44.71
Li	14	24	8	8	22	1	52	15	19	2	10	24	11	15	2	11	48
Ni	14.09	3.57	7.55	4.91	183.83	4.23	4.96	3.79	86.38	7.38	77.37	94.94	20.51	2.09	1.59	6.22	21.57
Sc	11.3	10	1.5	7.2	15	3.4	7.3	4	18.5	10.6	14.6	11.6	3.3	1.6	1.2	5.2	5.1
V	102.21	11.59	4.26	9.03	139.78	2.67	21.87	3.92	150.88	66	92.59	111.49	41.27	3.32		49.11	52.35
Zn	69.09	63.66	12	324	85.66	8.36	76.37	77.38	96.88	59.3	73.63	65.76	25.16	32.61	3.58	58.03	70.21
Ba	299.36	138.4	263.88	492.65	259.62	339.31	384.06	157.88	278.89	635.19	260.17	293.61	549.41	263.98	5.46	696.87	389.46
Cd	0.037	0.043	0.049	0.3	0.084	0.05	0.05	0.073	0.101	0.125	0.066	0.072	0.049	0.035		0.061	0.082
Cr	61.19	11.76	16.46	12.73	251.62	12.55	15.02	11.9	114.14	14.95	74.2	126.07	18.86	9.43	9.82	11.48	30.57
Ga	17.18	13.14	11.01	18.58	19.31	15.95	19.21	18.45	18.24	18.66	15.29	17.86	20.14	16.48	15.09	23.16	19.8
Mo	2.68	0.53	2.17	1.85	0.84	0.48	0.62	0.59	1.15	1.5	2.12	0.64	0.4	0.65	0.29	1.38	1.42
Pb	2.9	3.2	12.8	38.2	5.2	2.1	3.9	8.4	6.3	14.1	2.2	4.4	5.2	6.6	1.6	40	7.2
Sn	1.2	1.77	3.07	2.65	8.24	3.55	3.9	9.59	1.66	3.48	2.67	1.77	2.44	3.54	5.39	10	0.81
Tl	0.54	0.1		0.96	0.14	0.12	0.16	0.09	0.09	0.14	0.14	0.18	0.43	0.14	0.02	0.29	0.23
W	0.56	0.25	0.66	0.55	0.58	0.42	1	0.68	0.22	0.66	0.18	0.34	0.57	0.79	0.81	3.79	0.29

APPENDIX 1 *(Cont.)*

Number	R-38	R-41	R-42	R-43	R-44	R-45	R-46	R-47	R-48	R-50	R-51	R-52	R-53	R-54	R-55	R-56	R-57
Zone	17	17	17	17	17	17	17	17	17	17	18	18	18	18	17	17	17
UTME	633686	656675	670257	685822	695000	695018	691184	692819	690587	642978	305709	299515	305403	311479	637049	634211	620877
UTMN	5424766	5419254	5405392	5409034	5479820	5479815	5485776	5482091	5479711	5520033	5507623	5514904	5512540	5516571	5379247	5378698	5388093
SiO_2 (wt %)	76.14	64.02	61.06	82.32	68.87	72.39	62.68	79.73	70.62	67.35	73.39	78.48	65.88	65.19	71.15	70.22	73.01
Al_2O_3	13.97	18.25	14.86	9.89	12.32	13.45	16.15	11.6	12.2	13.09	11.41	9.61	10.59	12.65	10.94	13.43	12.73
TiO_2	0.36	0.32	0.81	0.12	0.45	0.53	0.52	0.09	0.41	0.49	0.3	0.26	0.64	0.89	0.31	0.6	0.28
Fe_2O_3	0.27	3.21	7	1.58	5.16	3.17	6.36	1.52	5.16	3.76	5.8	4.37	12.62	10.33	6.73	2.05	3.9
MgO	0.27	2.15	4.57	0.07	3.27	0.44	1.92	0.2	2.59	1.02	1.1	2.26	6.34	1.57	2.12	0.21	1
MnO		0.04	0.11	0.03	0.07	0.06	0.12	0.04	0.09	0.08	0.07	0.05	0.05	0.1	0.14	0.08	0.06
K_2O	8.32	1.67	1.75	1.94	1.55	1.84	0.75	2.15	1.96	4	3.48	0.75	0.05	0.55	2.43	1.21	1.61
CaO		4.27	5.18	0.21	0.94	0.73	3.25	0.55	1.19	3.17	0.87	0.09	0.13	3.33	0.08	2.96	1.87
Na_2O	0.12	4.5	4.28	3.31	2.33	4.22	5.88	2.06	2.29	1.36	2.24	2.62		4.46	0.17	5.41	3.74
P_2O_5	0.03	0.09	0.17	0.02	0.08	0.11	0.1	0.02	0.07	0.15	0.05	0.03	0.12	0.2	0.07	0.15	0.06
LOI	1.18	1.66	1.18	0.91	5.45	2.85	2.6	2.13	2.91	5.53	1.79	1.78	4.11	1.19	6.64	3.13	2.83
Total	100.66	100.18	100.96	100.41	100.48	99.78	100.34	100.11	99.5	99.99	100.51	100.3	100.53	100.46	100.78	99.46	101.08
Ce (ppm)	47.56	20.06	34.71	50.1	24.32	33.06	26.29	61.59	47.3	36.72	91.73	89.41	42.13	66.84	30.11	40.01	64.22
Cs	1.446	2.022	1.446	0.484	0.988	1.565	0.244	0.469	0.343	1.06	1.36	0.119	0.032	0.127	0.336	0.958	0.448
Dy	3.541	0.696	3.564	13.305	2.643	3.288	1.642	7.256	9.099	4.417	20	20	16.529	16.961	1.741	2.723	4.424
Er	2.041	0.316	2.083	8.892	1.713	1.983	0.906	4.851	5.991	2.833	18.213	13.791	11.067	11.104	1.036	1.567	2.686
Eu	1.078	0.634	1.111	1.134	0.568	0.798	0.765	0.654	1.731	0.938	3.344	3.097	2.054	2.625	0.353	1.084	1.212
Gd	4.247	1.159	3.807	10.257	2.564	3.388	2.125	6.291	8.168	4.248	20	18.172	13.243	15	2.103	3.326	5.047
Hf	7.2	2.8	3.7	10	5.8	4.8	3.2	6.6	7.6	4.5	17.7	15.5	10.2	12	4.4	4	6.4
Ho	0.677	0.122	0.719	2.94	0.566	0.66	0.323	1.579	1.949	0.94	5.817	4.464	3.596	3.606	0.348	0.535	0.898
La	21.06	11.14	15.68	21.62	10.85	14.98	12.62	26.39	20.43	16.53	35.54	34.47	16.2	25.11	13.85	17.7	29.49
Lu	0.341	0.041	0.295	1.327	0.267	0.305	0.13	0.723	0.903	0.424	2.79	1.926	1.643	1.678	0.161	0.23	0.409
Nb	11.8	1.7	7.5	23.1	8.3	6.1	3.8	9.1	10.9	8.4	28.2	24.6	15.9	20.3	5.4	5.9	9.8
Nd	22.85	8.96	18.11	28.45	13.3	16.66	12.52	30.18	28.41	18.69	63.72	61.97	31.5	45.84	14.1	20.3	29.68
Pr	5.767	2.396	4.417	6.569	3.136	4.12	3.186	7.648	6.447	4.539	13.472	12.999	6.39	9.835	3.633	5.057	7.708
Rb	93.4	69.11	42.61	54.36	25.87	40.6	15.44	40.23	34.89	79.52	79.04	13.2	0.72	6.41	33.6	31.74	35.5
Sm	4.85	1.58	3.92	7.69	2.9	3.54	2.47	6.45	7.03	4.1	17.54	16.03	9.35	12.56	2.58	3.95	5.94
Sr	21.3	602.4	138.5	32	49.4	72.9	138	29.2	32.7	43.9	49.1	24.5	2.7	58.3	20.4	93.3	60.8
Ta	0.99	0.26	0.62	1.66	0.72	0.61	0.43	0.88	0.85	0.77	1.82	1.64	1.12	1.45	0.59	0.59	0.87
Tb	0.639	0.145	0.595	1.962	0.428	0.536	0.297	1.107	1.405	0.698	3.886	3.161	2.467	2.633	0.297	0.48	0.759
Th	3.85	1.44	1.44	4.84	1.9	2.34	1.96	3.89	2.2	2.63	4.06	3.09	1.93	3.32	3.31	2.99	4.56
Tm	0.317	0.044	0.303	1.333	0.263	0.298	0.134	0.726	0.894	0.424	2.779	2.045	1.641	1.651	0.155	0.229	0.406
U	0.873	0.427	0.363	1.29	0.612	0.411	0.463	0.975	0.606	0.624	1.035	0.837	0.533	0.876	0.902	0.629	0.979
Y	16.82	3.32	19.79	79.81	14.76	17.37	8.84	44.95	52.92	25.98	120	115.18	95.35	96.46	9.5	13.5	24.7
Yb	2.2	0.28	1.96	8.74	1.73	2	0.87	4.84	5.91	2.8	18.26	13.31	10.78	11.01	1.06	1.52	2.69
Zr	274.6	113.7	155.4	332.6	216.7	183.1	127	202.6	288.6	178.6	688.8	565.8	375.6	460.4	167	157.3	257.2
Be	0.58	0.56	0.46	0.88	0.56	0.33	0.43	0.59	0.81	0.43	1.78	1.1		1.01	0.43	0.31	0.58
Co	0.78	5.66	24.83	0.25	9.06	4.53	16.76	0.41	7.74	7.08	0.91	0.28	9.89	13.2	9.2	1.62	3.2
Cu	2.67	4.53	40.23	18.12	8.01	14.98	7.18	12.35	29.15	6.36	5.86	10.06	30.14	12.26	49.01	2.5	1.96
Li	9	28	21	2	40	5	26	7	11	3	9	7	12	10	2	6	10
Ni	2.88	15.68	110.12	1.33	11.24	4.06	49.75	1.32	8.16	2.8	2.36	1.22	1.29	2.88	4.81	1.7	2.1
Sc	3.3	3.8	15.1	2.1	2.7	6.2	10.2	3.2	7.9	7.1	2.3	0.8	12.1	12.8	3.3	6.5	5.6
V	6.79	42.2	114.46	3.48	45.27	31.69	92.62	2.17	24.09	22.73	5.23	1.78	3.71	40.7	17.74	30.34	6.77
Zn	6.9	60.05	77.24	88.74	73.53	83.89	35.28	72.46	114.99	54.06	136.05	217	84.02	85.36	92.46	13.51	55.27
Ba	713.94	249.18	242.63	496.58	69.37	1101.27	204.97	223.05	306.06	266.72	543.24	45.02	25.85	140.86	433.61	273.7	212.71
Cd	0.05	0.036	0.07	0.119	0.066	0.057	0.044	0.114	0.063	0.062	0.204	0.145	0.075	0.097	0.084	0.031	0.062
Cr	10.44	31.07	84.66	8.71	15.54	8.75	64.7		21.33		10.1		8.12	8.45	9.08	8.18	8.26
Ga	19.34	23.43	15.72	12.75	17.94	16.65	17.68	16.09	20.75	17.17	32.23	19.84	28.46	23.33	14.16	15.72	15.07
Mo	0.7	2.62	0.83	3.25	1.12	0.54	0.32	0.93	1.39	0.35	1.77	1.09	5	0.81	1.06	0.37	0.22
Pb	2.6	5	1.6	5.4	4	12.1	1.2	11.4	3.9	2.2	4.7	3.8	0.8	1.3	8.3	2	2.5
Sn	3.49	0.7	1.58	4.31	2.46	1.41	1.71	2.63	2.66	2.09	10	5.68	3.58	2.08	1.75	1.31	2.09
Tl	0.24	1.04	0.08	0.08	0.12	0.25	0.08	0.13	0.14	0.12	1.18	0.16		0.02	0.16	0.09	0.12
W	0.45	0.42	0.18	0.93	0.27	0.27	0.32	0.27	0.25	1.77	0.72	0.37	0.71	0.23	0.68	0.29	0.23

APPENDIX 1 *(Cont.)*

Number	R-58	R-59	R-60	R-61	R-62	R-63	R-64	R-65	R-66	R-67	R-68	R-69	R-70	R-71	R-73	R-74	R-75
Zone	17	17	17	17	17	17	17	17	17	17	17	17	17	17	17	17	17
UTME	615919	617145	622270	622273	650653	650447	652983	657343	654526	634177	631020	630318	627893	626000	624067	646573	647630
UTMN	5387853	5386548	5383127	5383134	5382153	5381949	5383580	5392084	5391921	5342561	5341497	5342283	5342497	5349906	5351508	5346168	5347494
SiO_2 (wt %)	75.9	72.28	66.74	63.77	70.29	79.63	75.72	71.43	70.89	67.35	70.29	78.58	83.18	81.88	72.92	70.88	72.83
Al_2O_3	9.27	12.09	15.44	13.81	7.62	10.13	12.19	12.85	11.13	10.23	14.42	10.71	9.18	11.34	12.6	13.26	11.55
TiO_2	0.25	0.29	0.5	0.58	0.13	0.13	0.28	0.33	0.22	0.33	0.33	0.34	0.2	0.43	0.26	0.38	0.26
Fe_2O_3	6.99	2.69	3.87	5.46	13.49	3.84	3.62	3.14	9.76	5.91	5.22	2.17	0.96	0.51	4.88	6.2	7.12
MgO	0.81	0.34	1.79	3.26	4.08	2.64	1.31	0.59	1.88	0.75	0.61	0.25	0.24	0.45	0.83	0.28	1.01
MnO	0.18	0.08	0.06	0.07	0.14	0.01	0.04	0.05	0.09	0.19	0.09	0.03	0.01		0.13	0.03	0.22
K_2O	0.8	0.87	0.66	1.28	0.24	1.95	0.84	0.36	0.9	1.05	3.1	0.39	0.08	3.32	1.22	3.53	0.22
CaO	1.72	2.82	1.22	4.21	0.02	0.02	0.13	2	0.71	5.96	1.29	0.91	0.32	0.19	0.97	0.07	1.05
Na_2O	2.01	5.63	7.82	4.38		0.22	4.52	6.65	2.45	3.1	3.6	5.61	5.17	0.52	4.98	0.62	4.32
P_2O_5	0.04	0.06	0.09	0.1	0.02	0.02	0.05	0.07	0.05	0.07	0.05	0.06	0.03	0.05	0.04	0.08	0.04
LOI	2.76	2.9	1.57	2.94	5.08	2.4	1.47	2.15	2.05	5.6	1.24	0.36	0.4	1.57	1.04	4.14	1.93
Total	100.74	100.06	99.78	99.88	101.13	100.98	100.16	99.63	100.13	100.53	100.25	99.41	99.76	100.26	99.87	99.46	100.53
Ce (ppm)	47.09	62.39	47.45	20.81	47.67	43.47	47.84	48.86	33.49	33.67	48.8	56.95	39.26	29.93	54.58	8.6	74.67
Cs	0.145	0.268	0.097	0.424	0.062	0.331	0.137	0.173	0.279	0.484	2.961	0.134	0.091	1.083	0.246	0.754	0.164
Dy	3.929	4.74	4.008	1.717	3.785	3.882	3.482	4.048	2.007	5.793	8.957	6.58	5.79	13.308	10.992	3.06	9.443
Er	2.38	2.767	2.338	0.971	2.171	2.395	2.059	2.351	1.229	3.684	6.078	4.503	4.061	10.048	7.454	2.294	5.935
Eu	1.465	1.06	1.087	0.618	0.462	0.546	1.045	0.924	0.479	1.29	1.687	1.145	0.708	0.699	1.55	0.478	2.28
Gd	4.025	5.081	4.373	1.941	4.125	3.93	3.829	3.953	2.24	5.322	7.87	5.948	4.692	8.822	9.264	1.773	9.472
Hf	4.9	6	5.8	2.4	3.9	5.3	5.1	5.1	4.6	4.5	7.5	6.4	5.5	8.9	8.2	4.2	6.6
Ho	0.806	0.957	0.805	0.335	0.761	0.789	0.703	0.824	0.41	1.226	1.952	1.437	1.285	3.079	2.384	0.717	1.956
La	21.18	28.81	19.87	9.95	22.79	19.76	22.55	22.34	14.91	14.41	21.22	29.62	16.35	10.67	22	3.53	34.93
Lu	0.351	0.407	0.353	0.139	0.294	0.381	0.308	0.351	0.207	0.579	0.97	0.704	0.666	1.601	1.158	0.392	0.951
Nb	8.7	9.7	8	3.6	4.5	8	6.8	7.2	6	7.9	12.6	11.1	9.8	14.9	13.5	8.8	16.8
Nd	22.52	28.54	22.88	9.92	22.02	20.25	22.75	22.34	14.63	19.26	28.82	26	21	22.58	32.49	4.67	38.21
Pr	5.711	7.456	5.772	2.526	5.599	5.256	5.817	5.848	3.876	4.412	6.593	6.642	5.145	4.764	7.369	1.122	9.297
Rb	13.23	22.51	7.64	22.38	4.16	31.95	15.6	7.94	18.43	25.56	64.97	8.05	1.58	56.28	25.18	56.8	5.09
Sm	4.43	5.64	4.8	2.07	4.48	4.28	4.4	4.44	2.73	4.8	7.22	5.81	4.82	6.82	8.25	1.26	8.93
Sr	38.1	81.7	97.5	136.8	4.8	7.6	39.9	104.4	46.3	126.8	169.5	79.9	57.3	18.8	82.7	13.9	31.6
Ta	0.75	0.88	0.77	0.44	0.56	0.78	0.76	0.69	0.64	0.63	0.93	0.89	0.79	1.05	0.99	0.69	1.14
Tb	0.64	0.798	0.674	0.29	0.629	0.626	0.588	0.656	0.338	0.906	1.39	1.03	0.841	1.837	1.638	0.396	1.515
Th	3.22	4.4	4.02	1.42	2.95	4.12	3.16	3.47	3.26	1.71	3.21	3.43	3.2	2.11	2.75	1.9	2.78
Tm	0.352	0.407	0.35	0.14	0.312	0.362	0.302	0.351	0.194	0.554	0.925	0.677	0.636	1.597	1.14	0.372	0.894
U	0.78	1.066	0.987	0.357	0.753	0.985	0.785	0.851	0.839	0.432	0.836	0.877	0.838	0.59	0.744	0.577	0.715
Y	22.07	26.88	22.73	9.11	20.4	21.38	18.86	22.67	10.9	33.24	52.45	40.13	34.52	81.72	62.8	19.19	53.92
Yb	2.28	2.69	2.31	0.92	2.01	2.45	2.01	2.27	1.34	3.74	6.26	4.51	4.24	10.66	7.52	2.5	6.06
Zr	197.9	230.1	234.5	96	152.4	200.9	201	197.3	181.2	180.2	283.9	249.4	212.9	306.8	310.5	169.9	248.7
Be	0.4	0.62	0.53	0.5		0.28	0.3	0.27	0.44	0.38	0.79	0.42	0.24	0.15	0.68	0.22	0.52
Co	5.21	2.45	8.15	19.1	15.36	6.33	3.07	3.82	10.15	2.5	2.35	2.11	0.78	0.71	3.85	6.01	0.53
Cu	17.81	3.39	27.32	37.66	38.32	1.78	2.75	5.25	27.09	5.02	109.92	38.59	225	13.78	71.83	104.99	20.59
Li	9	3	7	12	15	11	13	5	9	7	17	5	3	4	5	3	20
Ni	0.94	2.19	12.28	57.01	3.35	1.3	1.34	3.19	5.06	1.33	1.27	1.43	0.96	1.84	3.14	2.15	1.21
Sc	5.2	4.8	7.9	11.1	3.8	4.2	6	5	2.2	11.9	13.8	8.4	4.1	7.6	13.1	7.4	10.8
V	3.21	10.75	50.15	116.42	6.13	1.48	2.48	10.98	11.39	4.16	5.13	4.41	1.6	1.81	1.5	15.46	1.8
Zn	81.06	44.98	48.67	64.9	126.81	25.64	32.61	39.04	55.08	63.29	85.77	31.62	28.06	18.36	78.75	5000	225
Ba	134.02	175.54	188.61	420.12	39.82	299.83	180.76	85.86	201.72	179.61	872.24	164.31	35.91	441.29	482.89	340.36	47.83
Cd	0.059	0.047	0.106	0.036	0.065	0.041	0.044	0.036	0.062	0.041	0.107	0.05	0.037	0.084	0.071	0.3	0.141
Cr		8.64	16.14	92.27	8.12		8.12	9.06	10.14		8.07		8.39	8.91	11.34	9.08	
Ga	12.04	15.46	16.7	15.36	12.05	14.29	14.73	13.09	16.07	13.82	20.46	11.29	9.26	7.98	18.61	15.34	22.01
Mo	2.37	0.31	0.93	0.64	2.8	0.72	0.66	0.3	1	0.87	0.37	0.36	0.71	0.94	1.69	0.98	3.38
Pb	3.3	3.3	3.3	13.1	1.3	1.4	1.9	1.5	4.9	1.3	3.5	4.5	1.3	3	1.3	9.4	3.2
Sn	1.09	2.26	2.1	1.34	0.92	2.17	1.77	1.32	1.77	1.15	2.57	7.9	1.58	0.93	2.73	2.56	3.51
Tl	0.04	0.07	0.05	0.14	0.02	0.21	0.06	0.04	0.06	0.08	0.29	0.05		0.68	0.08	0.52	0.04
W	0.26	0.3	0.25	0.24	0.58	0.52	0.22	0.38	0.21	0.38	0.42	0.29	0.41	0.73	0.3	0.44	1.88

APPENDIX 1 *(Cont.)*

Number	R-76	R-77	R-78	R-79	R-80	R-81	R-83	R-84	R-85	R-88	R-89	R-90	R-92	R-93	R-95	R-96	R-97
Zone	17	17	17	17	17	17	17	17	17	17	17	17	17	17	17	17	17
UTME	646889	651001	652251	649609	645584	648033	655360	650991	652434	669310	662609	654355	642730	641207	629641	623607	620443
UTMN	5347743	5347863	5350159	5347769	5350329	5344213	5361370	5366108	5371275	5358894	5358869	5358411	5351864	5357028	5360526	5358232	5365459
SiO_2 (wt %)	72.95	74.28	70.49	72.79	70.95	73.92	76.05	61.94	73.96	64.15	76.42	77.4	55.75	73.25	72.65	74.88	73.59
Al_2O_3	11.33	11.56	10.36	10.72	12.55	9.61	10.92	17.16	13.25	15.06	10.16	11.26	16.33	12.46	12.26	11.56	12.54
TiO_2	0.25	0.33	0.28	0.23	0.45	0.21	0.2	0.84	0.22	0.56	0.3	0.25	1.03	0.25	0.26	0.23	0.31
Fe_2O_3	5.43	2.08	3.99	5.23	4.71	1.69	2.18	6.23	2.92	4.71	3.21	1.49	9.03	4.35	3.95	3.5	4.4
MgO	0.85	0.57	2.4	2.19	1.24	0.1	0.33	3.17	0.8	2.79	1.14	0.09	4.76	1.18	0.57	0.18	0.86
MnO	0.08	0.03	0.13	0.27	0.08	0.13	0.03	0.08	0.02	0.08	0.05	0.04	0.13	0.06	0.06	0.1	0.07
K_2O	0.29	1.09	1.2	2.73	1.51	0.33	0.63	1.51	4.78	2.2	1.53	3	1.13	2.1	0.61	4.07	1.36
CaO	1.26	2.67	3.08	0.92	2.01	4.62	1.34	2.6	0.68	4.25	2.53	0.55	6.37	1.6	1.53	3.04	1.1
Na_2O	4.98	4.42	2.9	1.12	3.97	5.03	5.74	3.88	1.27	3.6	2.29	4.64	5.09	3.61	5.38	1.67	4.56
P_2O_5	0.04	0.06	0.07	0.04	0.08	0.04	0.05	0.13	0.03	0.16	0.07	0.05	0.14	0.03	0.05	0.04	0.07
LOI	1.66	2.9	5.49	3.95	2.93	3.59	1.9	2.69	2.37	1.7	2.55	0.4	1.62	1.51	1.88	0.71	1.23
Total	99.12	100	100.4	100.18	100.48	99.27	99.38	100.23	100.3	99.27	100.24	99.17	101.4	100.39	99.19	99.97	100.09
Ce (ppm)	54.47	34.09	55.45	46.98	41.67	47.96	56.87	32.93	80.22	55.88	59.27	96.91	23.31	57.15	40.86	55.77	62.08
Cs	0.126	0.72	0.652	1.405	0.336	0.3	0.344	1.239	2.351	1.62	1.234	0.322	0.199	0.621	0.163	0.331	0.263
Dy	9.573	5.297	7.018	7.707	6.233	8.247	6.45	4.561	7.764	2.513	7.69	11.053	2.808	10.843	8.584	9.912	13.25
Er	6.328	3.513	4.986	5.151	4.152	4.694	4.316	2.931	5.052	1.328	5.388	7.346	1.626	7.112	5.803	6.677	8.979
Eu	1.964	0.857	1.274	1.707	1.141	1.978	1.24	1.19	1.298	1.352	1.155	1.168	0.953	1.892	1.306	1.801	1.885
Gd	8.526	4.718	7.315	7.198	5.814	7.62	6.147	4.309	7.926	3.679	6.761	10.046	3.019	9.387	6.909	8.823	11.846
Hf	6.5	5.5	6.7	6.3	6.9	4.6	7.3	4	9.3	3.3	6.8	8.1	2.7	8.4	6.8	7.9	7.5
Ho	2.054	1.139	1.504	1.682	1.342	1.669	1.392	0.965	1.642	0.475	1.684	2.368	0.565	2.31	1.888	2.151	2.868
La	23.29	15.94	22.5	19.82	17.73	20.43	26.19	14.08	35.67	26.81	26.89	46.2	10.11	24.33	16.69	22.96	25.94
Lu	0.985	0.551	0.916	0.82	0.693	0.58	0.721	0.446	0.817	0.185	0.886	1.161	0.23	1.109	0.885	1.07	1.422
Nb	15	10.1	15.3	14.5	12.2	10.7	11.4	8.1	16.5	4.4	12.7	17.7	4.8	14.7	11.6	13.6	14
Nd	31.49	17.7	32.5	27.75	23.83	28.66	28.25	18.45	41.03	27.71	30.13	46.25	12.81	33.28	23.95	33.1	39.62
Pr	7.264	4.23	7.504	6.313	5.548	6.481	7.027	4.33	10.242	7.015	7.319	11.713	2.998	7.639	5.483	7.557	8.62
Rb	6.52	32.78	23.25	38.5	22.68	8.06	8.61	26.46	110.9	64.81	36.49	38.1	20.28	48.97	15.14	76.9	24.44
Sm	7.95	4.32	7.94	6.86	5.56	6.92	6.06	4.18	8.44	4.98	6.57	9.72	2.86	8.1	5.79	8	10.32
Sr	68.2	46.1	58.2	24.6	55.8	36.1	53.2	149.1	20.6	741.2	38.1	24.6	185.8	113.1	56.4	108.5	76.3
Ta	1.05	0.77	1.18	1.02	0.96	0.77	0.89	0.64	1.38	0.43	0.98	1.29	0.45	1.02	0.86	0.98	1.01
Tb	1.481	0.821	1.15	1.223	0.978	1.309	1.021	0.711	1.253	0.472	1.158	1.736	0.47	1.673	1.279	1.52	2.076
Th	2.66	3.13	3.97	2.64	3.85	1.95	3.51	2.11	6.5	3.51	5.08	5.8	1.22	3.12	2.5	2.81	3.28
Tm	0.966	0.547	0.799	0.794	0.644	0.653	0.68	0.445	0.77	0.186	0.856	1.151	0.236	1.079	0.879	1.031	1.398
U	0.691	0.875	1.004	0.686	1.02	0.434	0.845	0.554	1.525	1.028	1.213	1.289	0.314	0.836	0.696	0.717	0.846
Y	55.77	30.61	41.39	40.67	35.45	44.76	38	25.38	44.09	12.93	45.71	63.39	14.9	62.65	51.02	56.71	74.46
Yb	6.42	3.63	5.67	5.3	4.36	4.05	4.53	2.92	5.15	1.22	5.78	7.7	1.52	7.13	5.72	6.9	9.28
Zr	249.4	217.3	223.2	232.3	266.7	168.2	301.6	155.7	351.6	127.4	247.2	272.8	108	323.9	258	298.7	248.6
Be	0.41	0.24	0.55	0.6	0.47	0.3	0.18	0.56	1.22	0.82	0.54	0.44	0.39	0.89	0.64	0.61	0.66
Co	2.16	2.7	3.88	0.28	5.06	0.67	2.36	23.04	2.89	20.59	3.02	0.86	31.38	1.18	1.69	0.77	2.07
Cu	247	10.04	3.6	2.54	8.27	9.42	8.64	21.24	47.32	44.7	23.65	21.43	79.9	3.9	9.2	2.95	3.33
Li	17	9	9	10	11	3		23	13	42	11	2	5	8	7	2	6
Ni	1.28	1.98	2.35	1.22	2.28	1.4	1.95	52.22	6.92	90.08	2.08	1.82	48.72	1.11	1.13	1.54	1.26
Sc	10	5.9	5.3	8.1	9.9	6.6	5.9	15.5	8	10.5	6.8	5.4	19.3	10.9	10.6	10.4	10.9
V	1.76	11.16	15.7	2.94	16.1	2.73	2.97	158.34	15.39	94.29	10.72	9.11	224.45	2.7	2.63	2.67	4.74
Zn	58.65	19.1	75.08	120.59	61.25	17.43	303	67.48	49.24	71.88	46.78	27.43	125.33	55.63	32.36	26.07	71.46
Ba	73.47	114.88	271.09	578.29	289.55	38.1	148.47	371.41	381.1	936.66	315.97	502.76	262.58	872	98.83	673.17	315.08
Cd	0.155	0.066	0.09	0.054	0.053	0.056	0.281	0.04	0.09	0.075	0.074	0.058	0.095	0.074	0.048	0.059	0.06
Cr					10.21	8.12		60.94	12.3	154.66		8.02	66.88				
Ga	16.94	13.46	14.51	18.1	15.9	8.18	9.84	19.75	20.36	17.2	12.36	14.16	19.19	20.72	17.35	23.38	19.23
Mo	1.67	0.28	0.84	1.29	0.59	0.49	1.17	0.57	4.96	1.13	0.58	0.84	0.32	0.8	0.97	0.4	0.32
Pb	3.4	1.5	1.6	3.2	1.3	2.7	40	1.7	2.2	9.1	5	2.2	9.5	2.2	0.8	3.9	2
Sn	1.2	1.42	1.14	1.26	1.4	1.16	4.5	1.09	3.28	1.09	3.41	4.8	1.6	1.52	2.4	2.79	3.52
Tl	0.03	0.16	0.09	0.08	0.04	0.02	0.59	0.11	0.47	0.46	0.12	0.17	0.14	0.19	0.06	0.14	0.09
W	0.38	0.18	0.22	0.54	0.26	0.23	0.27	0.19	3.2	0.34	0.18	0.29	0.14	0.26	0.69	0.21	0.24

APPENDIX 1 *(Cont.)*

Number	R-99	R-100	R-101	R-102	R-103	R-104	R-105	R-106	R-107	R-108	R-109	R-110	R-111	R-112	R-113	R-114	R-115
Zone	17	17	17	17	17	17	17	18	18	18	18	18	18	18	18	18	18
UTME	647642	682691	690128	690120	690141	690131	691000	415336	485960	531686	534514	532847	565339	565322	563604	283202	283202
UTMN	5358250	5347877	5347240	5347192	5347379	5347279	5347500	5483070	5431392	5495949	5499618	5524237	5513155	5513845	5512701	5446802	5446202
SiO_2 (wt %)	80.52	70.41	69.93	72.06	66.46	72.45	76.92	63.43	76.59	62.62	74.42	77.15	69.32	73.08	74.66	68.7	74.4
Al_2O_3	9.15	13.12	15.88	14.03	14.98	11.65	12.03	11.52	13.29	15.75	13.83	10.29	12.7	12.42	10.87	14.35	10.82
TiO_2	0.12	0.36	0.25	0.32	0.62	0.22	0.17	0.35	0.1	0.57	0.06	0.19	0.39	0.45	0.16	0.36	0.22
Fe_2O_3	1.8	3.85	2.32	1.87	3.94	1.5	0.95	9.19	0.5	5.71	0.48	3.53	4.16	4.56	7.83	3.45	1.37
MgO	0.54	0.41	1.16	0.58	1.71	0.83	0.43	1.44	0.01	3.55	0.35	0.47	0.23	0.97	2.09	0.87	0.42
MnO	0.04	0.09	0.06	0.06	0.11	0.07	0.03	0.37		0.09	0.02	0.05	0.09	0.05	0.03	0.07	0.03
K_2O	2.04	4.02	4.37	2.91	1.74	1.45	3.09	1.02	1.25	1.44	3.01	2.22	2.43	0.72	1.79	4.43	2.1
CaO	1.41	2.58	1.51	2.87	4.68	4.23	1.75	11.64	0.39	4.61	1.32	1.92	3.48	1.34		2.35	3.95
Na_2O	1.99	0.22	1.81	2.55	1.91	3.63	1.98	1.07	5.83	3.87	3.94	1.03	3.06	5.18	0.24	0.33	2.15
P_2O_5	0.03	0.05	0.04	0.08	0.15	0.06	0.04	0.08	0.06	0.12	0.03	0.03	0.06	0.09	0.02	0.1	0.08
LOI	2.11	3.5	2.29	2.19	3.42	3.4	2.51	0.77	0.68	2.22	2.11	3.18	3.91	1.34	2.56	4.06	3.82
Total	99.76	98.6	99.63	99.53	99.73	99.48	99.9	100.88	98.71	100.55	99.56	100.04	99.84	100.21	100.24	99.06	99.36
Ce (ppm)	68.14	117.46	89.68	92.37	81.43	49.54	72.78	53.77	32.63	35.51	19.91	68.75	93.73	134.56	5.38	42.07	38.34
Cs	1.539	0.536	6.636	2.815	2.713	1.615	2.875	0.196	0.567	0.937	0.917	0.941	0.218	0.123	0.202	2.699	1.336
Dy	10.377	7.791	3.228	3.664	4.174	2.462	2.143	5.989	1.515	2.369	1.177	8.923	15.543	20	20	1.461	3.091
Er	7.238	4.701	2.213	2.31	2.753	1.799	1.496	3.987	1.037	1.428	0.746	6.078	10.528	13.548	19.709	0.766	2.34
Eu	1.274	1.923	0.837	1.307	1.472	0.484	0.687	1.387	0.334	0.799	0.317	1.086	1.91	2.518	1.137	0.604	0.962
Gd	9.256	7.994	3.407	4.281	4.838	2.48	2.433	6.43	1.251	2.715	1.252	8.353	13.829	20	13.616	2.134	2.96
Hf	8.3	7.4	4.2	4.7	4.3	3.1	3.1	6.5	3.3	3.7	2.2	6.9	12.1	10.7	16.6	3.8	6.8
Ho	2.278	1.577	0.691	0.744	0.882	0.548	0.454	1.29	0.327	0.484	0.245	1.964	3.434	4.55	5.993	0.272	0.706
La	28.27	56.29	48.08	46.86	39.58	25.43	40.73	23.04	10.78	17.34	8.44	29.24	38.46	54.06	1.26	20.71	17.53
Lu	1.245	0.718	0.447	0.413	0.486	0.374	0.296	0.695	0.182	0.212	0.128	0.967	1.68	1.953	3.019	0.114	0.419
Nb	18.7	15.6	14.8	14.3	8.2	11.3	11.4	11.8	7.4	7.1	11	14.7	26.2	28.4	45.8	6.4	6.4
Nd	38.67	52.51	30.64	36.98	36.5	19.24	23.86	28.97	8.16	15.71	7.59	36.24	54.2	81.77	9.75	16.65	17.02
Pr	9.145	13.921	9.315	10.288	9.586	5.489	7.38	6.954	2.357	4.07	2.312	8.826	12.586	18.395	1.281	4.659	4.464
Rb	33.99	81.33	138.05	85.22	51.63	58.52	91.68	18.54	26.99	39.48	63.68	38.31	47.14	13.02	22.98	89.26	75.28
Sm	8.94	9.78	4.51	5.96	6.44	3.23	3.4	6.5	1.45	2.96	1.53	8.14	12.65	19.54	7.08	2.77	3.19
Sr	18.1	14.1	117.2	179.1	236.2	194	106.6	52.8	108.6	226.3	86.5	98.5	85.7	84.8	13.4	37.8	93.4
Ta	1.38	1.04	1.27	1.09	0.62	0.98	1.05	0.9	0.88	0.7	1	1.04	1.63	1.76	2.94	0.7	1.02
Tb	1.6	1.275	0.531	0.625	0.711	0.389	0.362	0.996	0.232	0.398	0.196	1.39	2.401	3.41	3.291	0.277	0.475
Th	3.73	15	13.86	11.97	9.77	9.85	10.79	3.61	7.23	3.46	1.8	4.97	5.32	5.87	6.97	2.66	4.9
Tm	1.156	0.721	0.365	0.362	0.435	0.304	0.243	0.618	0.166	0.208	0.12	0.939	1.641	2.009	3.05	0.112	0.371
U	0.891	3.891	3.338	2.711	2.251	2.476	2.724	0.859	2.119	0.992	0.729	1.197	1.193	1.261	1.545	0.774	1.295
Y	60.25	41.49	19.91	20.55	24.82	16.6	13.11	35.86	9.99	13.19	7.67	53.91	90.32	120	120	7.75	19.8
Yb	7.88	4.81	2.68	2.57	3.02	2.21	1.76	4.33	1.16	1.37	0.8	6.3	10.98	13.06	19.96	0.75	2.6
Zr	293.5	302.7	154.5	197.7	174.5	116.7	113.9	257.6	102.3	145.3	48.6	236.4	443.6	367	477.6	142.7	250.6
Be	0.47	0.85	1.02	0.94	0.63	0.6	0.71	0.44	0.68	0.51	0.75	0.72	1.21	1.26	0.85	0.57	0.39
Co	3.59	15.39	1.91	1.85	6.64	2.4	0.69	12.42	0.34	20.1	0.16	3.23	2.55	5.03	9.4	10.86	2.18
Cu	2.79	58.98	15.18	3.38	13.21	25.1	5.34	10.92	1.8	43.54	1.92	9.42	1.86	3.54	2.71	187	44.76
Li	2	3	26	16	16	12	9	2	4	22	3	12	6	6	7	2	6
Ni	2.46	1.51	1.5	2.19	2.43	1.98	0.97	18.27	1.23	66.6	1.18	2.34	1.61	5.74	1.79	7.8	5.35
Sc	4.9	6.1	3.4	4.3	8.9	3	2.3	7.9	0.8	11.2	1	4.2	8	7.7	1.7	4.5	2.2
V	5.67	6.46	16.81	9.59	59.87	12.96	9.84	22.03	1.9	99.24	1.75	3.59	6.13	16.04	1.31	45.2	10.93
Zn	11.84	29.32	26.34	45.75	54.69	29.1	17.29	143.67	18.5	66.56	17.2	68.17	54.7	47.53	24	27.27	23.7
Ba	200.03	834.09	770.95	596.12	695.2	332.89	578.8	80.4	264.95	293.35	611.59	367.53	550.06	245.23	361.75	200.14	199.08
Cd	0.069	0.092	0.044	0.064	0.072	0.048		0.094		0.045		0.064	0.101	0.073	0.083	0.118	0.096
Cr					8.09	8.19				126.93				9.15		14.81	11.2
Ga	11.73	18.04	15.92	14.54	15.63	10.01	10.82	15.26	17.27	18.05	15.22	14.48	21.42	20.79	25.07	16.98	10.47
Mo	0.22	0.32	1.26	0.24	0.59	0.64	0.33	0.47	0.45	0.51	0.14	2.83	0.46	0.28	0.22	0.98	0.53
Pb	1.6	4.4	7.9	7.6	14.5	9.3	5.1	12.8	6.3	3	2.1	4.1	2.1	2.1	2.1	3.3	2
Sn	1.49	5.87	1.12	1.46	1.58	0.99	0.79	2.59	2.61	1.8	1.34	2.48	2.88	3.34	10	1.04	0.72
Tl	0.08	0.15	0.22	0.21	0.45	0.15	0.19	0.15	0.12	0.15	0.3	0.13	0.13	0.03	0.06	0.6	0.61
W	0.1	1.68	0.58	1.1	0.52	0.36	0.33	0.36	0.61	0.3	0.18	0.24	0.23	0.16	0.99	0.98	0.35

APPENDIX 1 *(Cont.)*

Number	R-116	R-117	R-118	R-119	R-120	R-121	R-122	R-123
Zone	18	17	17	17	17	17	17	17
UTME	313280	647800	647800	707947	630000	628000	627080	628025
UTMN	5330673	5519200	5519500	5358713	5468000	5471000	5474000	5475000
SiO_2 (% wt)	69.04	83.36	79.13	84.15	83.38	78.24	72.6	73.36
Al_2O_3	15.55	5.49	5.72	8.59	4.65	10.51	12.61	12.92
TiO_2	0.46	0.11	0.11	0.18	0.12	0.13	0.32	0.39
Fe_2O_3	2.79	4.93	5.51	0.43	6.23	1.98	3.43	3.68
MgO	1.07	0.55	5.54	0.05	2.57	1.69	4.33	1.91
MnO	0.03		0.1		0.04	0.02	0.06	0.05
K_2O	1.58	1.8	0.05	4.19	0.04	3.66	2.98	3.95
CaO	0.73		0.24	0.41	0.01	0.27	0.06	0.04
Na_2O	6.31	0.17	0.11	1.62	0.02	0.72	0.33	0.23
P_2O_5	0.34	0.02	0.03	0.03	0.02	0.02	0.05	0.03
LOI	1.31	3.35	2.9	0.41	1.79	3.27	4.07	3.72
Total	99.21	99.8	99.44	100.08	98.88	100.51	100.86	100.28
Ce (ppm)	85.17	43.31	24.72	127.65	9.54	74.04	56.53	42.54
Cs	0.799	0.446	0.034	0.26	0.022	1.369	0.768	1.392
Dy	8.776	2.762	1.75	7.793	1.71	5.133	3.463	3.444
Er	5.759	1.563	1.13	5.19	1.09	3.471	2.174	2.108
Eu	1.686	1.938	0.59	2.007	0.19	0.457	0.894	0.825
Gd	10.355	3.52	1.955	9.364	1.341	5.635	4.05	3.445
Hf	8	2.7	2.8	8.8	2.1	6.2	6.2	6
Ho	1.857	0.548	0.369	1.658	0.363	1.085	0.716	0.705
La	33.92	21.03	11.73	54.34	4.24	34.45	25.7	18.85
Lu	0.972	0.236	0.194	0.816	0.16	0.555	0.327	0.334
Nb	12.4	5.1	4.4	13.8	3.1	12.2	11	9.8
Nd	51.67	20.11	11.04	62.21	4.63	30.75	24.86	19.4
Pr	11.78	5.206	2.859	15.781	1.148	8.445	6.604	5.094
Rb	35.7	33.47	1.24	42.33	0.94	92.22	56.65	66.88
Sm	11.9	4.03	2.22	12.11	1.06	6.2	4.7	3.74
Sr	110	3.5	5	104.5	1.4	12.3	14.2	52.5
Ta	0.81	0.54	0.47	1.08	0.41	1.39	1.02	0.9
Tb	1.482	0.502	0.288	1.326	0.25	0.86	0.595	0.557
Th	5.01	1.97	1.93	5.11	1.38	8.54	4.07	2.92
Tm	0.894	0.234	0.18	0.799	0.16	0.539	0.32	0.322
U	1.202	0.612	0.467	1.195	0.427	2.183	1.163	1.218
Y	51.5	14.56	10.34	42.49	10.28	29.58	19.77	19.73
Yb	6.11	1.55	1.23	5.3	1.06	3.68	2.16	2.16
Zr	300.4	101.9	111.2	313.7	86.1	177.6	237.3	238.1
Be	0.93	0.38	0.24	0.38		0.87	0.6	1.19
Co	2.6	7.31	6.54	1.77	12.59	1.76	3.73	5.87
Cu	167	115.66	111.21	6.35	14.53	4.72	2.92	27.85
Li	18	4	16	5	10	10	13	4
Ni	5.23	4.52	1.04	5.28	9.24	3.97	2.04	2.76
Sc	14.8	2.7	3.4	4.5	2.4	2.3	3.3	3.7
V	21.26	4.57	2.82	4.57	8.94	2.07	14.64	45.41
Zn	104.7	2790	1559	74.35	40.07	31.79	36.68	374
Ba	317.34	257.56	9.52	177.33	6.66	203.23	161.29	245.47
Cd	0.231	0.3	0.3	0.299		0.043	0.04	0.3
Cr	15.25	9.32						8.09
Ga	15.79	5.59	13.71	13.51	6.46	13.55	14.63	19.58
Mo	0.63	0.88	0.34	5	0.47	0.86	0.68	3.92
Pb	12.4	40	40	22.3	0.5	2.1	2.4	5.7
Sn	2.68	1.16	1.8	3.42	1.91	3.67	7.27	10
Tl	0.26	2	0.06	0.43		0.18	0.21	0.86
W	0.42	1.17	0.38	0.31	0.4	0.44	1.4	3.07

Projection = NAD 83

APPENDIX 2

Mineralogy of Felsic Volcanic Rocks as Determined from Thin Section

			Phenocrysts			Alteration Pl			Matrix								
Sample	District	Group	Qz	Pl	Tot	Chl	Ser	Car	Qz-Pl	Chl	Ser	Car	Epi	Hbl	Bio	Zir	Op
R-2003-1	Quévillon	FI	10	15	25		10-100		50	6	12	6					1
R-2003-2	Quévillon	FI	2		2				64	0.5	18	5	0.5				10
R-2003-3	Quévillon	FI		15	15		15		20	15	35						15
R-2003-4	Quévillon	FIIIa	4	2	6	5	0.5		70	5	15	1	1				2
R-2003-5	Quévillon	FIIIa							83	4	10.5		0.5				2
R-2003-8	Quévillon	FIIIa	4	5	9		5	5	15	15	57	3					1
R-2003-9	Quévillon	FIIIa	1	2	3		3	3	87		7	3					
R-2003-10	Val-d'Or	FII							80	1	15						4
R-2003-11	Val-d'Or	FII							60	18		20	2				
R-2003-12	Val-d'Or	FII															
R-2003-13	Val-d'Or	FIIIa															
R-2003-14	Val-d'Or	FII															
R-2003-15	Val-d'Or	FII							28	34	34	1					3
R-2003-16	Val-d'Or	FII	1	1	2		10		70	10	10	6					2
R-2003-17	Val-d'Or	FII															
R-2003-18	Val-d'Or	FII							52		28						20
R-2003-19	Val-d'Or	FII ?							64	8	17			10			1
R-2003-20	Val-d'Or	FII							69		30		1				
R-2003-116	Val-d'Or	FII		2	2	0-10	20-70	0-7	75	5	15	1					2
R-2003-21	NVZ-Ext	FII							73		19						8
R-2003-22	NVZ-Ext	FII							34		34	31					1
R-2003-23	NVZ-Ext	FII															
R-2003-25	NVZ-Ext	FII	2	2	4		3-25	20	67		26	2					1
R-2003-26	NVZ-Ext	FII	10	10	20		20	10-70	42	12	20	5					1
R-2003-27	NVZ-Ext	FII		3	3				86	10			1				
R-2003-28	NVZ-Ext	FII															
R-2003-29	NVZ-Ext	FII		5	5	10		90	75	15			2				3
R-2003-30	NVZ-Ext	FII		1	1	90			30	39		10	20				
R-2003-31	NVZ-Ext	FII	1	3	4		3	20	47	13	23	10					3
R-2003-32	NVZ-Ext	FII		10	10	0-10	10	0-2	53	1	20	15					1
R-2003-37	NVZ-Ext	FII							90	5	5						
R-2003-42	NVZ-Ext	FII	0.5	1	1.5		30		33	15	25	3	0.5	11	11		
R-2003-43	NVZ-Ext	FII	0.5		0.5				89.5		7						3
R-2003-34	Normétal	FIIIa							40		59						1
R-2003-35	Normétal	FIIIa							81		13	6					
R-2003-36	Normétal	FII							80	5	15						
R-2003-38	Normétal	FII															
R-2003-44	Joutel	FII															
R-2003-45	Joutel	FII	1	3	4		6	10	70		11	12					3
R-2003-46	Joutel	FI	1	3	4	5-20	15		69	10	15	1					1
R-2003-47	Joutel	FIIIa	3		3				64		30						3
R-2003-48	Joutel	FIIIa	10	4	14		2	10-80	52	15	15	3					1
R-2003-51	Matagami	FIIIb	0.5	0.5	1		3		65	8	10	10					6
R-2003-52	Matagami	FIIIb	0.5		0.5	3	3		75.5	16	3						5
R-2003-53	Matagami	FIIIb							51	47							2
R-2003-54	Matagami	FIIIb		70	70				5	20							5
R-2003-55	Hunter	FII	6		6		100		67		15	10					2
R-2003-56	Hunter	FII	0.5		0.5		2	5	71	0.5	15	10					3
R-2003-57	Hunter	FII	2	10	12		5	10	63	5	15	3					2
R-2003-58	Hunter	FII	1	1	2	5	3-10	2	71	12	10	3					2
R-2003-59	Hunter	FII	1	6	7		5	10-70	73	5	3	9					3
R-2003-60	Hunter	FII	1	15	16	0-15	3	0-98	52	18		6					8
R-2003-61	Hunter	FII	3	17	20	0-80	0-95		13	51	6						10
R-2003-62	Hunter	FII	0.5		0.5				61.5	19		17					2
R-2003-63	Hunter	FII	1		1				82	5	10					1	1
R-2003-64	Hunter	FII		3	3		0-100		76	15	3						3
R-2003-65	Hunter	FII	5	15	20		10	5-15	55	10	5	5					5
R-2003-66	Hunter	FII	3		3				51	20	13	7				5	1
R-2003-108	Chibougamau	FI		15	15	20		60	25	18		35	7				
R-2003-109	Chibougamau	FI	1	3	4		20	1	81.5		7	7					0.5
R-2003-110	Chibougamau	FII ?							52.5	5	37	0.5					5
R-2003-111	Chibougamau	FIIIa	2	2	4	1	3	7	20	7	60	7					2
R-2003-112	Chibougamau	FIIIa	4	10	14	1	10	3	61.5	10	10	1.5					3
R-2003-113	Chibougamau	FIIIa	4		4				65.5	20	10						0.5
R-2003-50	Selbaie	FII	0.5	0.5	1		25	5	20		68	5					6
R-2003-117	Selbaie	FII	3		3		100		65	1	30						1

APPENDIX 2 *(Cont.)*

			Phenocrysts			Alteration Pl			Matrix								
Sample	District	Group	Qz	Pl	Tot	Chl	Ser	Car	Qz-Pl	Chl	Ser	Car	Epi	Hbl	Bio	Zir	Op
R-2003-118	Selbaie	FII	0.5		0.5				65	33		1					0.5
R-2003-67	Noranda	FIIIa	Tr						62	15	6	12					5
R-2003-68	Noranda	FIIIa	0.5	3	3.5		40	3	33.5	8	47	6					2
R-2003-69	Noranda	FIIIa	0.5	2	2.5		3	3	81.5	3	2	7					4
R-2003-70	Noranda	FIIIa	1	2	3				91.5	2		1		0.5			2
R-2003-71	Noranda	FIIIa							67		31						2
R-2003-72	Noranda	FIIIa							82	10	7						1
R-2003-73	Noranda	FIIIa		1	1	20		15	52	26		19					2
R-2003-74	Noranda	FIIIa ?	0.5		0.5				54.5	2	38						5
R-2003-75	Noranda	FIIIa	5	1	6	10	5-65	2	70	20	3						1
R-2003-76	Noranda	FIIIa	6	3	9	5	15	3	75	8	3	3					2
R-2003-77	Noranda	FIIIa							75	6	15	2					2
R-2003-78	Noranda	FIIIa	1		1	5	5	90	75.5	6	10	7					0.5
R-2003-79	Noranda	FIIIa	7		7				60	7	15	10					1
R-2003-80	Noranda	FIIIa		0.5	0.5		2-10	0-10	82.5	1	7	6					3
R-2003-81	Noranda	FIIIa							79	2	5	12					2
R-2003-82	Noranda	FIIIa	1	24	25	10		90	15	15		40	5				
R-2003-83	Noranda	FIIIa		0.5	0.5		3	0.5	84.5		4	6					5
R-2003-84	Noranda	FIIIa	1	1	2	65	12		13	64.5	12	3	0.5				5
R-2003-88	Noranda	FIIIa	9	1	10		38	2	65	8	6	7		3			1
R-2003-89	Noranda	FIIIa	0.5	0.5	1	1	5		40	5	50	2					2
R-2003-90	Noranda	FIIIa	0.5	1	1.5			3	88	5	1	2.5					2
R-2003-92	Noranda	FIIIa ?		33	33	5	80	5	20	15		10		15			7
R-2003-93	Noranda	FIIIa															
R-2003-95	Noranda	FIIIa															
R-2003-96	Noranda	FIIIa	7	3	10	1	1	2	60.5	25		3		1			0.5
R-2003-97	Noranda	FIIIa	8	15	23	3	10	3	49	12	12	2					2
R-2003-98	Noranda	FIIIa	3	77	80	5	5	0.5		9	3	1					7
R-2003-99	Noranda	FIIIa	3	0.5	3.5	5	2		71.5	2	7	15					1
R-2003-100	Bousquet	FI	0.5		0.5				68	0.5	25	3					3
R-2003-101	Bousquet	FI	5	10	15	3	20	10	50	3	24	3			5		
R-2003-102	Bousquet	FI							50.5	3	40	1		0.5			5
R-2003-103	Bousquet	FI															
R-2003-104	Bousquet	FI	4	5	9		22	1	60	5	20	5					1
R-2003-105	Bousquet	FI	3	10	13		5-10	6-10	71.5	1	10	3.5		0.5			0.5
R-2003-41	NVZ-ext	FI	15	10	25		3-60		48	10	10		7				
R-2003-85	Kinojevis	FII	5	2	7		4	0.5	77.5		15						0.5
R-2003-106	Coniagas	FII	0.5	1	1.5		1	3	25	15	0.5	55.5		0.5			2
R-2003-107	Lac Hébert	FI	10	10	20		7		68.5	0.5	9				0.5	0.5	1
R-2003-114	NVZ-int	FI	3		3				51		35	5					6
R-2003-115	NVZ-int	FI	0.5		0.5				53	2	25	19					0.5
R-2003-119	Marbridge	FII							93.5	1	3				2		0.5

Notes: Phenocryst >0.5 mm; abbreviations: Bio = biotite, Car = carbonate, Chl = chlorite, Epi = epidote, Hbl = hornblende, Op = opaque, Pl = plagioclase, Qz = quartz, Ser = sericite, Zir = zircon